ment has led us to believe that the osteoclast apoptosis can be a good therapeutic target to develop efficient drugs for pathological bone loss, and therefore, the molecular mechanism of the osteoclast apoptosis has attracted a great deal of attention.

Guanosine triphosphate (GTP)-binding proteins (G-proteins) regulate cellular function by interconverting between the GTP-binding (active) form and the guanosine diphosphate (GDP)-binding (inactive) form. Small G-proteins are monomeric G-proteins with molecular weight of 20–30 kDa, and to date, >100 members have been identified. Recent studies have revealed that small G-proteins can be targets of nitrogen-containing bisphosphonates.[5] It has been shown that these bisphosphonates inhibit post-translational prenylation of small G-proteins, which may be a mechanism of their action to induce osteoclast apoptosis. Rho, Rac, and Cdc42 are members of Rho family small G-proteins,[6] and accumulating evidence has shown that they mediate growth factor receptor signaling and regulate the cytoskeletal organization in various types of cells.[7,8] Recent studies, however, have revealed that some members of Rho family small G-proteins, especially Rac1, also mediate anti-apoptotic signals in some types of cells, such as hematopoietic cells, cerebellar granule neurons, and COS7 cells.[9–11] RhoA and Rac1 are reported to be required for the cytoskeletal organization and bone-resorbing activity of osteoclasts, but their roles in the osteoclast survival and function are not fully elucidated.

In this study, with the adenovirus vector expression system, we investigated the role of RhoA, Rac1, and Cdc42 in osteoclast survival and function. Among them, we found that Rac1 is critical for both osteoclast survival and bone resorption, and we showed that Rac1 lies downstream of M-CSF receptor signaling, mediates the survival signaling of osteoclasts through phosphatidylinositol 3-kinase (PI3K)-Akt pathways, and plays an important role in bone-resorbing activity, probably by regulating osteoclast membrane movement.

MATERIALS AND METHODS

Animals and chemicals

Treatment of each animal was conducted in accordance with the Guide for Animal Experimentation established at our institute. Newborn ddY mice and 5-week-old male ddY mice were purchased from Sankyo Laboratories Animal Center. α-MEM and DMEM were purchased from GIBCO BRL and Life Technologies (Rockville, MD, USA), and FBS was purchased from Sigma Chemical (St Louis, MO, USA). Bacterial collagenase was purchased from Wako Pure Chemical (Tokyo, Japan) and dispase from Godo Shusei Co. (Tokyo, Japan). Prostaglandin E_2 (PGE_2) was obtained from Sigma Chemical, and 1α,25-dihydroxyvitamin D_3 [$1\alpha,25(OH)_2D_3$] was purchased from Calbiochem (La Jolla, CA, USA). Type I collagen gel was purchased from Nitta Gelatin (Osaka, Japan). MEK inhibitor PD98059 was purchased from Cell Signaling Technology (Beverly, MA, USA), PI3K inhibitor LY294002 was purchased from Sigma Chemical, and wortmannin and rapamycin were obtained from Calbiochem. Recombinant mouse M-CSF was obtained from R&D Systems (Minneapolis, MN, USA). Anti-GFP antibody (JL-8) was obtained from Clontech (Palo Alto, CA, USA), anti-Rac1 and anti-ERK were from Transduction Laboratories (Lexington, KY, USA), anti-phospho-ERK was from New England Biolabs (Beverly, MA, USA), and anti-phospho Akt (S473) and anti-Akt were from Cell Signaling Technology. Other chemicals and reagents used in this study were of analytical grade.

Osteoclast culture

Osteoclast-like cells (OCLs) were generated in the mouse co-culture system as described previously.[12,13] Briefly, mouse primary osteoblastic cells from 1-day-old ddY mouse calvaria and bone marrow cells from tibias of 5-week-old male ddY mice were co-cultured on 10-cm plastic dishes or collagen gel–coated dishes with 10% FBS containing α-MEM in the presence of 10 nM $1\alpha,25(OH)_2D_3$ and 1 mM PGE_2. On day 4 or 5, when OCLs began to appear, mouse co-cultures were incubated with a small amount of α-MEM containing adenovirus vectors for 1 h at 37°C. The cells were washed twice with PBS and further incubated with α-MEM/10%FBS at 37°C. Twenty-four hours after adenovirus infection, collagen gel was digested with 0.2% collagenase, and co-cultured cells were reseeded onto dentin slices or plastic dishes. For Western blotting and the survival assay, OCLs were purified following a modified method originally reported by Tezuka et al.[14] In brief, osteoblasts and stromal cells were removed with α-MEM containing 0.1% collagenase and 0.2% dispase 4–8 h after reseeding.

Adenovirus construction

Every cDNA of fusion protein of enhanced green fluorescent protein (EGFP) and dominant negative mutant of RhoA (T19N, $RhoA^{DN}$), Rac1 (T17N, $Rac1^{DN}$), and Cdc42 (T17N, $Cdc42^{DN}$), or constitutively active Rac1 (G12V, $Rac1^{CA}$) gene cloned in pCAGGS vector was a kind gift from Dr Michiyuki Matsuda (Research Institute for Microbial Diseases, Osaka, Japan).[15] Adenovirus vectors carrying these cDNA was constructed using the in vitro ligation technique with a commercially available kit from Clontech. The adenovirus vector carrying only EGFP cDNA was used as a control vector. Adenovirus vector carrying the dominant negative mutant of Rac1 with CAG promoter was kindly provided by Yoh Takuwa (Kanazawa University, Japan). Adenovirus vector carrying cDNA of the myristoylated form of Akt (Akt^{CA}), which contains a Src myristoylation signal that promotes association with the plasma membrane causing constitutive activation through phosphorylation by Akt-activating kinases, was a generous gift from Dr Hideki Katagiri (Tohoku University).[16] Adenovirus vector carrying cDNA of a catalytic subunit p110α of PI3K was also kindly provided by Dr Hideki Katagiri.[17] To determine the multiplicity of infection (MOI) of the viruses, we used a modified endpoint cytopathic effect assay as previously described.[18]

Pit formation assay

The pit formation assay was carried out as reported.[19] Briefly, OCLs obtained on a collagen gel co-culture system were recovered by digesting the gel as described above. An aliquot of the crude OCL preparation was transferred onto dentine slices (Wako Pure Chemical) and cultured for an additional 8 h. To prevent the effect of OCL survival on the pit formation assay, the assay was performed after 8 h. After the 8-h incubation, the medium was removed, and 1 M NH_4OH was added to the wells for 30 minutes. Adherent cells were removed from the dentine slices by ultrasonication, and the resorption pits were visualized by staining with 1% toluidine blue. The resorbed area was measured using an image analysis system (System Supply, Nagano, Japan) linked to a light microscope (Nikon, Tokyo, Japan).

Osteoclast survival assay

The survival rate of OCLs was measured as reported.[1,12] Briefly, OCLs were subjected to TRACP staining at 0, 12, and 24 h after purification. Cell viability/survival rate was expressed as the proportion of morphologically intact $TRACP^+$ multinucleated cells. The number of viable cells remaining at the different time-points was shown as a percentage of the cells at time 0. To determine the effect of M-CSF or various inhibitors of signal transduction pathways on cell survival, each reagent was added to OCL cultures at time 0 after purification.

Western blotting

All extraction procedures were performed at 4°C or on ice. Cells were washed with ice cold PBS and lysed by adding TNE buffer (1% NP-40, 10 mM of Tris-HCl [pH 7.8], 150 mM of NaCl, 1 mM of EDTA, 2 mM of Na_3VO_4, 10 mM of NaF, and 10 μg/ml of aprotinin). The lysates were clarified by centrifugation at 15,000 rpm for 20 minutes. An equal amount of protein was subjected to 10% SDS-PAGE, transferred electrophoretically onto a nitrocellulose membrane, and probed sequentially with an appropriate primary antibody followed by a secondary antibody coupled with horseradish peroxidase (Promega, Madison, WI, USA). Immunoreactive proteins were visualized by enhanced chemiluminescence (ECL) Western blotting detection reagents (Amersham, Arlington Heights, IL, USA) following the procedure recommended by the supplier. The blots were stripped by incubating for 20 minutes in stripping buffer (2% SDS, 100 mM of 2-mercaptoethanol, and 62.5 mM of Tris-HCl [pH 6.7]) at 50°C and reprobed with other antibodies.

Determination of Rac1 and Cdc42 activation by M-CSF

Activation of Rac1 and Cdc42 in response to M-CSF was examined with a glutathione *S*-transferase (GST) pull-down assay using a commercially available Rac/Cdc42 activation assay kit (Upstate, Charlottesville, VA, USA). In brief, after adding 100 ng/ml M-CSF, total cell lysates of OCLs from 10-cm dishes were collected as described above at indicated time-points and incubated with p21-binding domain of PAK1 and GST fusion protein immobilized on glutathione agarose beads for 1 h at 4°C. Precipitates were subjected to 10% SDS-PAGE and immunoblotted with anti-Rac1 or anti-Cdc42 antibody.

Actin ring formation

Cells were first stained for TRACP to identify osteoclasts and then incubated for 30 minutes with rhodamine-conjugated phalloidin solution (Molecular Probes, Eugene, OR, USA).[20] The actin rings formed by osteoclasts were detected with a fluorescence microscope (Carl Zeiss, Oberkochen, Germany).

Quantification of osteoclast membrane movement with time-lapse video microscopy

The effect of $Rac1^{DN}$ expression on the dynamic cytoskeletal organization of OCLs was evaluated and quantified using time-lapse video microscopy as follows. After confirming the gene transduction to OCLs on collagen gel by detecting green fluorescence under a fluorescent microscope, the gel was digested, and OCLs infected by either EGFP or $Rac1^{DN}$ adenovirus were reseeded on serum-coated glass coverslips placed in 35-mm dishes. Three to 8 h later, when OCLs had fully spread, 50 ng/ml M-CSF was applied to the cultures. Recording of OCLs started 30 minutes before the M-CSF treatment and continued for 90 minutes using a phase contrast time-lapse video microscope (LVR-3000N and pxc930; Sony, Tokyo, Japan). Resulting moving images were transferred to a computer. Pairs of the first and the second cell images with a 5-minute interval in between were selected at 30 minutes or longer after M-CSF treatment, and the contours of the cell pairs were traced with photo-retouch software (Photoshop; Adobe). Each pair's second image was subtracted from its first image. Total number of pixels remaining after the subtraction of two serial static images were counted on the image analysis software (NIH image) and called the motile area. Motility was expressed as a percentage of the motile area to the first image. The measurement was performed on 20 pairs from four OCLs in $Rac1^{DN}$ and control virus.

Statistical analysis

Each series of experiments was repeated at least three times. The results obtained from a typical experiment were expressed as the means ± SD. Significant differences were determined using an unpaired *t*-test, the Mann-Whitney test, or a factorial ANOVA. Fisher's protected least significant difference (PLSD) or Dunnett test was used as a posthoc test.

RESULTS

Adenovirus vector-mediated gene transduction into OCLs

To analyze the role of Rho family small G-proteins in mature OCLs, we constructed adenovirus vectors carrying constitutively active Rac1 or dominant negative RhoA, Rac1, and Cdc42 fused with EGFP and infected OCLs with these viruses. First, we confirmed the efficiency of adenovirus vector-mediated gene transduction into OCLs 36 h

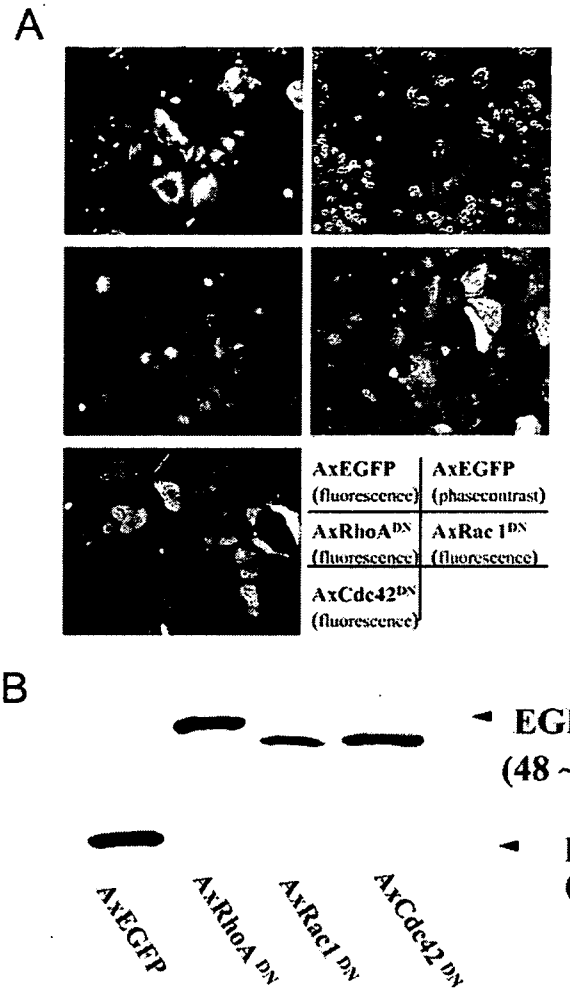

FIG. 1. Adenovirus vector-mediated gene expression in OCLs. The expression of EGFP, EGFP-RhoA^{DN}, EGFP-Rac1^{DN}, and EGFP-Cdc42^{DN} introduced into OCLs was confirmed 36 h after infection by (A) fluorescence microscopy and (B) Western blot analysis using anti-EGFP antibody. Most OCLs expressed EGFP or EGFP-fusion protein 36 h after infection. On Western blotting using anti-EGFP antibody, EGFP-Rho family small G-protein fusion protein was expressed as a molecule with molecular weight about 48–50 kDa.

after infection by fluorescence microscopy to detect EGFP fluorescence in situ and Western blot analysis using anti-EGFP antibody. Clear EGFP fluorescence was detected with a fluorescence microscope in almost 100% of the infected OCLs (Fig. 1A). Expression of fusion proteins of each dominant negative mutant and EGFP was observed as ~48-kDa molecular weight bands by Western blotting (Fig. 1B).

Effects of dominant negative mutants of Rho family small G-proteins on the activity and survival of OCLs

We examined the effect of Rho family small G-proteins mutants on pit-forming activity of OCLs and their survival. As shown in Fig. 2, RhoA^{DN} and Rac1^{DN} virus-infected OCLs showed a remarkable decrease in their bone-resorbing activity, whereas Cdc42^{DN} overexpression had no observable effect. In contrast, as shown in Fig. 3A, only Rac1^{DN} virus could significantly decrease their survival rate compared with the control virus, and RhoA^{DN} and Cdc42^{DN} viruses had no effect on their survival (Fig. 3). The survival rate of OCLs in EGFP virus–, RhoA^{DN} virus–, Rac1^{DN} virus–, and Cdc42^{DN} virus–infected cultures at 24 h was 35.7 ± 5.0%, 37.3 ± 3.5%, 24.0 ± 1.0%, and 41.7 ± 4.7%, respectively. These results clearly show that Rac1 signaling promotes osteoclast survival. Similar results were obtained using Rac1^{DN} adenovirus vector with CAG promoter (data not shown).

Rac1 lies downstream of M-CSF receptor and mediates an anti-apoptotic signal

M-CSF markedly enhances the survival of osteoclasts and causes their spread in vitro.[1,21] Because Rac1 is also known to regulate the cytoskeletal organization and induce cell spreading in some types of cells, we hypothesized that Rac1 might lie downstream of M-CSF receptor pathways and mediate signaling pathways essential for the survival and the cytoskeletal organization of osteoclasts. We first examined whether Rac1 was activated in OCLs in response to M-CSF treatment using the GST pull-down assay. As expected, Rac1 was activated immediately after application of M-CSF, and the activation was sustained for at least 10

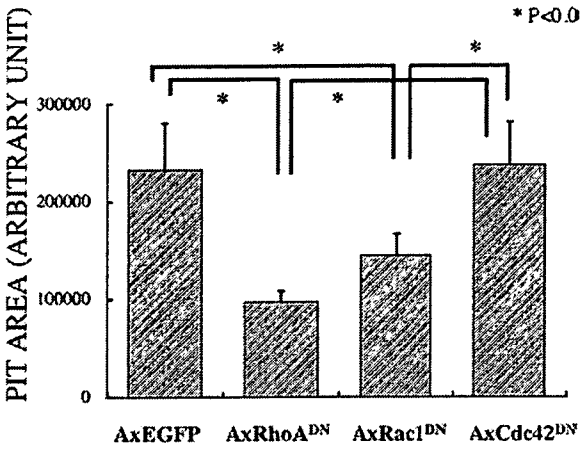

FIG. 2. Effect of dominant negative mutant of RhoA, Rac1, and Cdc42 expression on bone-resorbing activity of OCLs. Twenty-four hours after adenovirus infection, OCLs were collected and reseeded onto dentin slices. OCLs were removed 12 h later, and pits were visualized with 0.5% toluidine blue. Pit area was quantified with an image analysis system. Overexpression of $RhoA^{DN}$ and $Rac1^{DN}$ decreased bone resorptive activity of OCLs, whereas $Cdc42^{DN}$ had no significant effect.

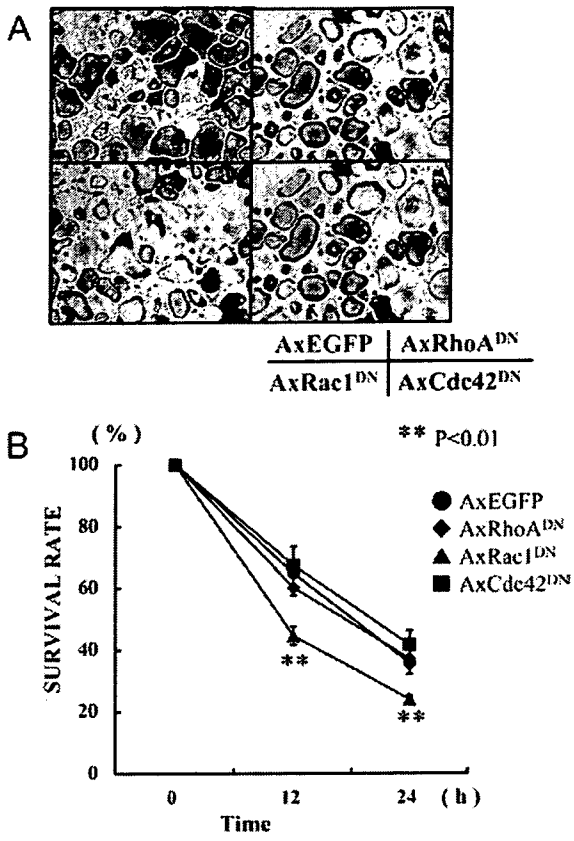

FIG. 3. Effect of dominant negative mutant of RhoA, Rac1, and Cdc42 expression on survival of OCLs. Twenty-four hours after adenovirus infection, OCLs were purified and cultured for an additional 24 h. (A) The survival of the cells after 24 h of purification was evaluated by TRACP staining. (B) After TRACP staining, viable OCLs were counted after 12 and 24 h of purification and expressed as a percentage of the cells at time 0. $Rac1^{DN}$-infected OCLs died significantly earlier than those in the control group, whereas Rho^{DN} and $Cdc42^{DN}$ had no effect on OCL apoptosis. Results represent the mean ± SD for a typical experiment among three independent experiments.

minutes (Fig. 4A). Next we studied the effect of $Rac1^{DN}$ overexpression on M-CSF–induced promotion of OCL survival. As shown in Fig. 4B, M-CSF clearly increased the survival of control virus–infected OCLs. $Rac1^{DN}$ overexpression not only suppressed the survival rate of OCLs at the basal level but also completely abrogated the pro-survival effects of M-CSF (Fig. 4B). In addition, the survival rate of $Rac1^{CA}$-infected OCL at 24 h after purification was significantly higher than that of control virus–infected OCLs, further confirming the role of Rac1 in OCL survival (Fig. 4C).

$Rac1^{CA}$ induced osteoclast survival and its survival signal of osteoclasts was mediated mainly through the PI3K/Akt pathway

To further clarify the role of Rac1 in the survival signal, we studied the downstream cascade of Rac1 signaling. We previously reported that the Ras/Erk pathway promotes osteoclast survival, whereas other groups described the anti-apoptotic function of the PI3K/Akt signaling pathway.[3,12] To determine whether these pathways contribute to the effects on cell survival by Rac1, we used specific inhibitors to these molecules. Figure 5A shows the effects of the inhibitors on OCL survival at 12 h after purification and addition of each reagent. The effect of $Rac1^{CA}$ on the promotion of OCL survival was blocked by either LY294002 or wortmannin but not significantly by PD98059 at this time-point, indicating the essential role of PI3K/Akt pathways downstream of Rac1. Mandatory activation of Akt pathways by overexpressing Akt^{CA} remarkably enhances OCL survival as shown in Fig. 5B, further confirming the anti-apoptotic role of these pathways. Consistent with these results, M-CSF–induced Akt phosphorylation was markedly suppressed by $Rac1^{DN}$, whereas $RhoA^{DN}$ and $Cdc42^{DN}$ had no effect (Fig. 5C). On the other hand, the activation of Erk as determined by anti-phospho-Erk antibody blotting was not affected by any of the mutants of three small G-proteins, as shown in Fig. 5D.

Rac1 and PI3K synergistically act downstream of M-CSF receptor signaling

These results suggest that Rac1 lies upstream of PI3K pathways, but there is a controversy with regard to the hierarchy of Rac1 and PI3K. Therefore, we further analyzed the relationship between Rac1 and PI3K activation downstream of M-CSF receptor pathways using specific inhibitors and adenovirus vectors. The activation of Rac1 in response to M-CSF treatment was not suppressed by LY294002 (Fig. 6A). Overexpression of a catalytic subunit of PI3K, p110, promoted the downstream effector Akt phosphorylation even in the absence of M-CSF, which was

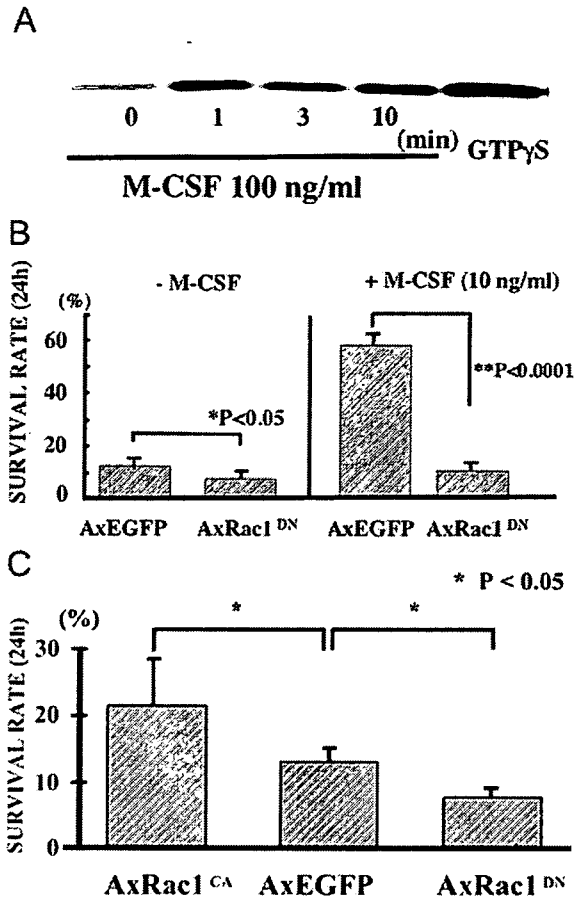

FIG. 4. Rac1 lies downstream of M-CSF signaling in OCLs. (A) After application of 100 ng/ml M-CSF, total cell lysates of OCLs from 10-cm dishes were collected at indicated time-points and incubated with p21-binding domain of PAK1 and glutathione *S*-transferase (GST) fusion protein immobilized on glutathione agarose beads for 1 h at 4°C. Precipitates were subjected to 10% SDS-PAGE and immunoblotted with anti-Rac1 antibody. (B) Purified adenovirus-infected OCLs were incubated for 24 h with or without 10 ng/ml M-CSF, and cell survival was assessed. Whereas M-CSF clearly increased OCL survival in control virus-infected OCLs, $Rac1^{DN}$ completely abrogated the M-CSF–induced survival. (C) The survival rate of $Rac1^{CA}$ virus-infected OCLs was significantly higher than that of control virus-infected cells, whereas $Rac1^{DN}$ expression promoted their apoptosis. Results represent the mean ± SD for a typical experiment among three independent experiments.

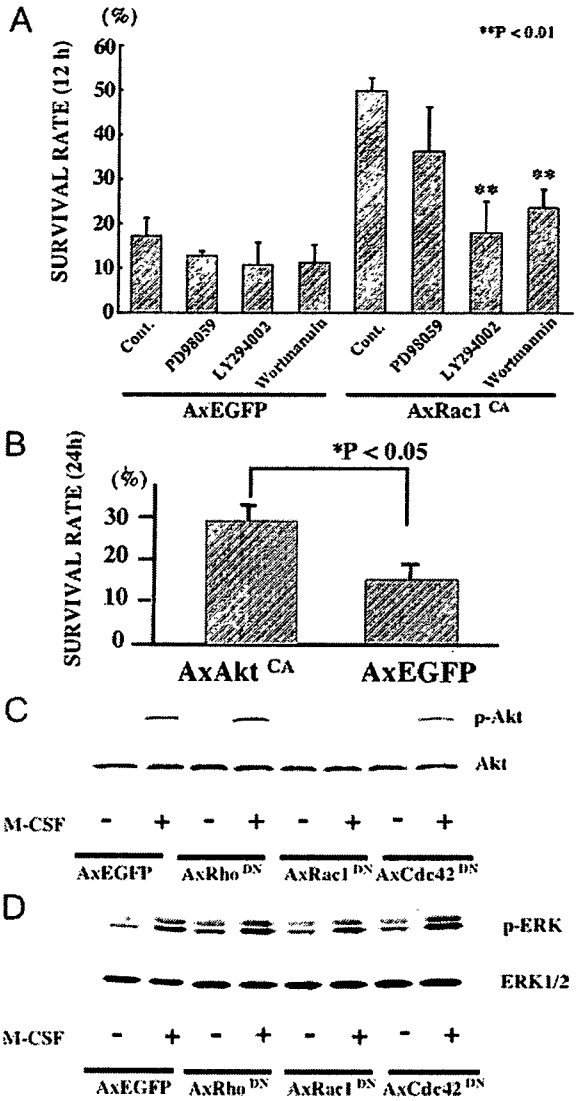

FIG. 5. Involvement of PI3K/Akt pathways on OCL survival. (A) Purified EGFP adenovirus– or $Rac1^{CA}$ adenovirus–infected OCLs were incubated for 12 h in the presence of one of the following inhibitors: PD98059 (40 μM), LY294002 (4 μM), or Wortmannin (100 nM). After TRACP staining, viable OCLs were counted, and the survival rate was expressed as a percentage of the cells at time 0. The effect of $Rac1^{CA}$ on the promotion of OCL survival was blocked by LY294002 and Wortmannin, but not significantly blocked by PD98059. (B) The active form of Akt (Akt^{CA}) was overexpressed in OCLs by adenovirus, and OCL survival was assayed. Akt^{CA} increased OCL survival about 2-fold to control virus-infected OCLs. (C and D) The effect of $RhoA^{DN}$, $Rac1^{DN}$, and $Cdc42^{DN}$ adenovirus on Akt and ERK activation was examined by Western blotting with anti-phospho-Akt or ERK antibody. M-CSF treatment stimulated both PI3K and Mek-Erk pathways within 5 minutes. The activation of Akt was abrogated only by $Rac1^{DN}$ (C), whereas these dominant negative mutants did not affect the phosphorylation of Erk (D). Results represent the mean ± SD for a typical experiment among three independent experiments.

partially blocked by co-expression of $Rac1^{DN}$ (Fig. 6B). These results suggest that Rac1 serves as both upstream and downstream effector of PI3K and that interaction between Rac1 and PI3K is important for the survival signaling of OCLs.

Rac1 overexpression does not affect actin ring formation in OCLs, but reduces M-CSF–induced cell spreading

We next examined the effect of Rac1 activation or inactivation on the cytoskeletal organization of OCLs. Unex-

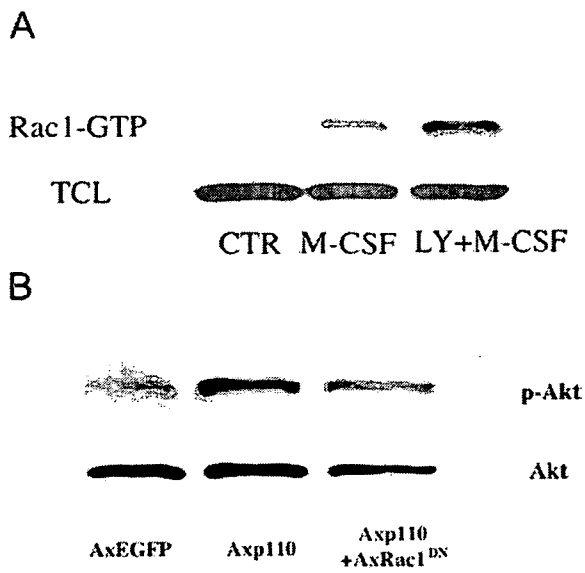

FIG. 6. Relationship between Rac1 and PI3K activation. The activation of Rac1 after 100 ng/ml M-CSF treatment with or without 20 μM LY294002 was examined by GST pull-down assay mentioned in Fig. 4A. The M-CSF–induced Rac1 activation was not suppressed by LY294002 (A), whereas enhancement of Akt phosphorylation by overexpression of catalytic subunit p110α of PI3K was partially blocked by coinfection of Rac1^{DN} (B).

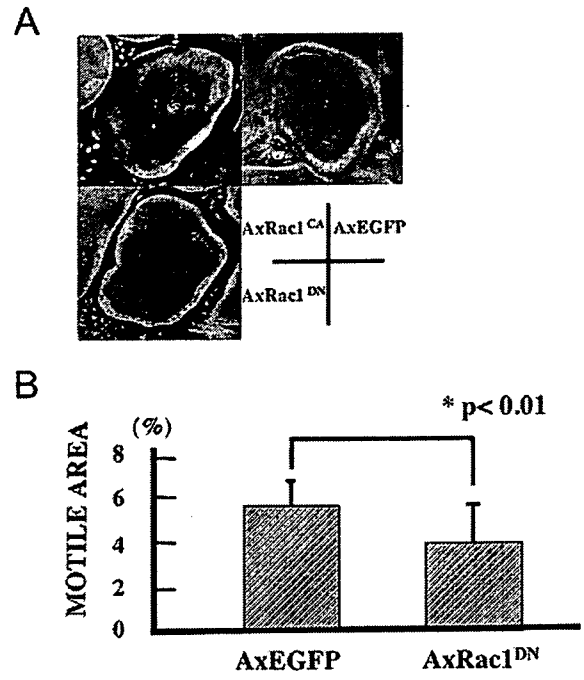

FIG. 7. Rac1 regulates the motility of OCLs. (A) EGFP or Rac1 mutant adenovirus-infected OCLs were incubated for 12 h after purification, and actin ring formation was visualized by rhodamine-phalloidin staining. No obvious difference in cytoskeletal organization was observed between mutated Rac1-expressed OCLs and control OCLs. (B) Before and after 50 ng/ml M-CSF treatment, OCLs expressing either EGFP or Rac1^{DN} were recorded with a time-lapse video microscope, and membrane movement was quantified with image analysis software. Results represent the mean ± SD of a typical experiment.

pectedly, however, as shown in Fig. 7A, we could not detect any obvious difference in actin ring formation between mutant Rac1 adenovirus-infected and control vector–infected OCLs in a static condition. All the OCLs were almost the same size and showed apparently normal actin ring formation. On the other hand, using time-lapse video microscopy, we found that overexpression of Rac1^{DN} dramatically reduced the membrane ruffling and spreading of the cells in response to 50 ng/ml M-CSF application as shown in Fig. 7B. Motile area of control virus– and Rac1^{DN}-infected OCLs was 5.7 ± 1.1% and 4.0 ± 1.7%, respectively ($p < 0.01$).

DISCUSSION

Rho family members are known to mediate various growth factor receptor signaling pathways and to regulate cytoskeletal organization of the cells.[8,22] Rac1 is a member of Rho family small G-proteins and is known to be a potent activator of actin polymerization and induce lamellipodia formation and surface membrane ruffling.[7] In addition to its role in the cytoskeletal organization, Rac1 is also known to be involved in the apoptosis signal. Whereas its pro-apoptotic function has been shown in some types of cells through JNK activation,[23–26] anti-apoptotic effects of Rac1 signaling have also been reported in other types of cells.[9–11,27] Moreover, the Rac1$^{-/-}$ embryos showed numerous programmed cell deaths in the space between the embryonic ectoderm and endoderm, leading to early embryonic lethality.[28] These results clearly indicate that Rac1 is implicated in the survival signals in various types of cells.

Nitrogen-containing bisphosphonates such as alendronate and risedronate are potent therapeutics of osteoporosis and suppress bone-resorbing activity of osteoclasts and induce their apoptosis. It has been proposed that nitrogen-containing bisphosphonates act on osteoclasts by inhibiting post-translational prenylation of Rho family small G-proteins. Zhang et al.[29] first described the importance of RhoA in osteoclast cytoskeletal organization and function using clostridium botulinum–derived ADP-ribosyltransferase (C3 exoenzyme). Similarly, using dominant active and negative mutant proteins of RhoA, Chellaiah et al.[30] reported that integrin-dependent activation of phosphoinositide synthesis, actin stress fiber formation, podosome reorganization for osteoclast motility, and bone resorption require Rho stimulation. Razzouk et al.[31] revealed that both Rac1 and Rac2 are involved in actin ring formation and the bone-resorbing activity of the cells by introducing anti-Rac1 or anti-Rac2 antibody into permeabilized osteoclasts. Ory et al.[32] showed that Rho and Rac worked antagonistically in avian multinucleated giant cells and that Rac activation promoted spreading of the cells. More recently, Faccio et al.[33] showed that RhoA and Rac1 lie downstream of the β3 integrin and are involved in the cytoskeletal organization of osteoclasts. These results suggest that RhoA and Rac1 critically regulate the cytoskeletal organization and function of osteoclasts.

In this study, using adenovirus vector-mediated gene transduction systems, we showed the essential role of Rac1 in bone-resorbing activity, survival, and motility of OCLs. Two major pathways have been reported to be involved in osteoclast survival signaling (i.e., the Mek/Erk pathway and the PI3K/Akt pathway). The effect of $Rac1^{CA}$ on the promotion of OCL survival was blocked by PI3K inhibitors but not by Mek inhibitors. M-CSF–induced phosphorylation of Akt was inhibited by $Rac1^{DN}$ expression but not by Rho^{DN} or $Cdc42^{DN}$ expression. In contrast, $Rac1^{DN}$ expression did not affect M-CSF–induced Erk phosphorylation, indicating that Rac1 is specifically involved in Akt activation downstream of M-CSF receptor pathways (Figs. 5C and 5D). These results clearly show that the prosurvival action of M-CSF on OCLs is mainly mediated by Rac1 and that Rac1 is important for M-CSF–dependent PI3K/Akt activation in OCLs. Lee et al.[3] also showed that TNF-α prolonged the survival of osteoclasts, which was abrogated by PI3K inhibitor. They also revealed the involvement of Grb2 and ceramide in TNF-α–induced Erk activation in osteoclasts.[3] However, contrary to these observations, Sugatani and Hruska[34] recently reported that silencing of Akt1 and/or Akt2 by small interfering RNA suppressed osteoclast differentiation but did not affect osteoclast survival. The reason for this discrepancy remains unknown, and further study is required to clarify the exact role of PI3K/Akt pathways in osteoclast survival. Recent studies have shown the involvement of mTOR (mammalian target of rapamycin) in osteoclast survival.[34,35] We also found that rapamycin strongly suppressed OCL survival in both the presence and absence of M-CSF (data not shown). The role of Rac1 on mTOR activation remains elusive, and further studies will be required.

Although our results suggest that Rac1 seems to act upstream of PI3K in OCLs and is consistent with some reports,[36,37] other studies have shown that Rac1 serves as downstream effector of PI3K.[38,39] Because many guanine-nucleotide exchange factors (GEFs) for Rac1 have been identified, and among them, members of the Vav, Sos, Tiam, PIX, SWAP-70, and P-Rex families have been suggested to be regulated by PI3K.[40] Furthermore, phosphatidylinositol 3,4,5-triphosphate, the endproduct of PI3K, can bind directly to Rac1 in vitro. In this study, we showed that PI3K inhibitor did not affect M-CSF–induced Rac1 activation (Fig. 6A), which means Rac1 lies upstream of PI3K. However, our results also indicate that Rac1 seems to act downstream of PI3K, because p110α-induced Akt phosphorylation was partially blocked by $Rac1^{DN}$ (Fig. 6B), and $Rac1^{CA}$ could not activate Akt by itself (data not shown). One possible explanation for these contradictory results is that Rac1 and PI3K act synergistically on cell survival or there is a positive feedback loop between Rac1 and PI3K activation, which may play an important role in the survival signaling of OCLs.

Finally, we examined the effect of Rac1 on the cytoskeletal organization of OCLs. Unexpectedly, however, there was no remarkable difference in actin ring formation between control OCLs and $Rac1^{DN}$ or $Rac1^{CA}$-infected cells (Fig. 7A). Because this is considered to be caused by the static condition in which we observed the cells, dynamic cytoskeletal rearrangement of OCLs in response to M-CSF treatment was examined using a video microscope. Suppression of Rac1 pathways by dominant negative mutant overexpression induced less membrane movement in response to M-CSF treatment compared with EGFP adenovirus–infected cells (Fig. 7B). Based on these observations, we concluded that Rac1 plays a crucial role in membrane movement of OCLs and that decreased bone resorption in $Rac1^{DN}$-infected OCLs is probably caused by the reduced motility of the cells.

In conclusion, small GTPase Rac1 is critically involved in M-CSF receptor signaling and mediates survival signaling of osteoclasts primarily by modulating the PI3K/Akt pathways. Rac1 also plays a significant role in bone resorptive activity of the cells, probably by regulating the motility of osteoclasts.

ACKNOWLEDGMENTS

The authors thank H Katagiri and T Asano for providing Mek^{CA}, myrAkt, and subunit p110αg of PI3K adenoviruses, Noriko Takuwa and Yoh Takuwa for dominant negative Rac1 adenovirus with CAG promoter, M Matsuda for dominant negative and constitutively active RhoA, Rac1, and Cdc42 constructs, and R Yamaguchi and M Ikeuchi for expert technical assistance. This work was supported in part by Grants-in-Aid from the Ministry of Education, Culture, Sports, Science and Technology of Japan and Health Science research grants from the Ministry of Health, Labour and Welfare of Japan to ST.

REFERENCES

1. Jimi E, Shuto T, Koga T 1995 Macrophage colony-stimulating factor and interleukin-1 alpha maintain the survival of osteoclast-like cells. Endocrinology **136**:808–811.
2. Lee ZH, Kim HH 2003 Signal transduction by receptor activator of nuclear factor kappa B in osteoclasts. Biochem Biophys Res Commun **305**:211–214.
3. Lee SE, Chung WJ, Kwak HB, Chung CH, Kwack KB, Lee ZH, Kim HH 2001 Tumor necrosis factor-alpha supports the survival of osteoclasts through the activation of Akt and ERK. J Biol Chem **276**:49343–49349.
4. Lee ZH, Lee SE, Kim CW, Lee SH, Kim SW, Kwack K, Walsh K, Kim HH 2002 IL-1alpha stimulation of osteoclast survival through the PI 3-kinase/Akt and ERK pathways. J Biochem (Tokyo) **131**:161–166.
5. Rogers MJ, Gordon S, Benford HL, Coxon FP, Luckman SP, Monkkonen J, Frith JC 2000 Cellular and molecular mechanisms of action of bisphosphonates. Cancer **88**(12 Suppl):2961–2978.
6. Hall A 1998 Rho GTPases and the actin cytoskeleton. Science **279**:509–514.
7. Ridley AJ, Paterson HF, Johnston CL, Diekmann D, Hall A 1992 The small GTP-binding protein rac regulates growth factor-induced membrane ruffling. Cell **70**:401–410.
8. Burridge K, Wennerberg K 2004 Rho and Rac take center stage. Cell **116**:167–179.
9. Linseman DA, Laessig T, Meintzer MK, McClure M, Barth H, Aktories K, Heidenreich KA 2001 An essential role for Rac/Cdc42 GTPases in cerebellar granule neuron survival. J Biol Chem **276**:39123–39131.
10. Nishida K, Kaziro Y, Satoh T 1999 Anti-apoptotic function of Rac in hematopoietic cells. Oncogene **18**:407–415.
11. Murga C, Zohar M, Teramoto H, Gutkind JS 2002 Rac1 and RhoG promote cell survival by the activation of PI3K and Akt,

independently of their ability to stimulate JNK and NF-kappaB. Oncogene **21**:207–216.
12. Miyazaki T, Katagiri H, Kanegae Y, Takayanagi H, Sawada Y, Yamamoto A, Pando MP, Asano T, Verma IM, Oda H, Nakamura K, Tanaka S 2000 Reciprocal role of ERK and NF-kappaB pathways in survival and activation of osteoclasts. J Cell Biol **148**:333–342.
13. Akatsu T, Tamura T, Takahashi N, Udagawa N, Tanaka S, Sasaki T, Yamaguchi A, Nagata N, Suda T 1992 Preparation and characterization of a mouse osteoclast-like multinucleated cell population. J Bone Miner Res **7**:1297–1306.
14. Tezuka K, Sato T, Kamioka H, Nijweide PJ, Tanaka K, Matsuo T, Ohta M, Kurihara N, Hakeda Y, Kumegawa M 1992 Identification of osteopontin in isolated rabbit osteoclasts. Biochem Biophys Res Commun **186**:911–917.
15. Itoh RE, Kurokawa K, Ohba Y, Yoshizaki H, Mochizuki N, Matsuda M 2002 Activation of rac and cdc42 video imaged by fluorescent resonance energy transfer-based single-molecule probes in the membrane of living cells. Mol Cell Biol **22**:6582–6591.
16. Fujishiro M, Gotoh Y, Katagiri H, Sakoda H, Ogihara T, Anai M, Onishi Y, Ono H, Funaki M, Inukai K, Fukushima Y, Kikuchi M, Oka Y, Asano T 2001 MKK6/3 and p38 MAPK pathway activation is not necessary for insulin-induced glucose uptake but regulates glucose transporter expression. J Biol Chem **276**:19800–19806.
17. Katagiri H, Asano T, Ishihara H, Inukai K, Shibasaki Y, Kikuchi M, Yazaki Y, Oka Y 1996 Overexpression of catalytic subunit p110alpha of phosphatidylinositol 3-kinase increases glucose transport activity with translocation of glucose transporters in 3T3-L1 adipocytes. J Biol Chem **271**:16987–16990.
18. Yamamoto A, Fukuda A, Seto H, Miyazaki T, Kadono Y, Sawada Y, Nakamura I, Katagiri H, Asano T, Tanaka Y, Oda H, Nakamura K, Tanaka S 2003 Suppression of arthritic bone destruction by adenovirus-mediated dominant-negative Ras gene transfer to synoviocytes and osteoclasts. Arthritis Rheum **48**:2682–2692.
19. Tamura T, Takahashi N, Akatsu T, Sasaki T, Udagawa N, Tanaka S, Suda T 1993 New resorption assay with mouse osteoclast-like multinucleated cells formed in vitro. J Bone Miner Res **8**:953–960.
20. Kanehisa J, Yamanaka T, Doi S, Turksen K, Heersche JN, Aubin JE, Takeuchi H 1990 A band of F-actin containing podosomes is involved in bone resorption by osteoclasts. Bone **11**:287–293.
21. Fuller K, Owens JM, Jagger CJ, Wilson A, Moss R, Chambers TJ 1993 Macrophage colony-stimulating factor stimulates survival and chemotactic behavior in isolated osteoclasts. J Exp Med **178**:1733–1744.
22. Ridley AJ, Hall A 1992 The small GTP-binding protein rho regulates the assembly of focal adhesions and actin stress fibers in response to growth factors. Cell **70**:389–399.
23. Aznar S, Lacal JC 2001 Rho signals to cell growth and apoptosis. Cancer Lett **165**:1–10.
24. Brenner B, Koppenhoefer U, Weinstock C, Linderkamp O, Lang F, Gulbins E 1997 Fas- or ceramide-induced apoptosis is mediated by a Rac1-regulated activation of Jun N-terminal kinase/p38 kinases and GADD153. J Biol Chem **272**:22173–22181.
25. Embade N, Valeron PF, Aznar S, Lopez-Collazo E, Lacal JC 2000 Apoptosis induced by Rac GTPase correlates with induction of FasL and ceramides production. Mol Biol Cell **11**:4347–4358.
26. Subauste MC, Von Herrath M, Benard V, Chamberlain CE, Chuang TH, Chu K, Bokoch GM, Hahn KM 2000 Rho family proteins modulate rapid apoptosis induced by cytotoxic T lymphocytes and Fas. J Biol Chem **275**:9725–9733.
27. Ruggieri R, Chuang YY, Symons M 2001 The small GTPase Rac suppresses apoptosis caused by serum deprivation in fibroblasts. Mol Med **7**:293–300.
28. Sugihara K, Nakatsuji N, Nakamura K, Nakao K, Hashimoto R, Otani H, Sakagami H, Kondo H, Nozawa S, Aiba A, Katsuki M 1998 Rac1 is required for the formation of three germ layers during gastrulation. Oncogene **17**:3427–3433.
29. Zhang D, Udagawa N, Nakamura I, Murakami H, Saito S, Yamasaki K, Shibasaki Y, Morii N, Narumiya S, Takahashi N 1995 The small GTP-binding protein, rho p21, is involved in bone resorption by regulating cytoskeletal organization in osteoclasts. J Cell Sci **108**:2285–2292.
30. Chellaiah MA, Soga N, Swanson S, McAllister S, Alvarez U, Wang D, Dowdy SF, Hruska KA 2000 Rho-A is critical for osteoclast podosome organization, motility, and bone resorption. J Biol Chem **275**:11993–12002.
31. Razzouk S, Lieberherr M, Cournot G 1999 Rac-GTPase, osteoclast cytoskeleton and bone resorption. Eur J Cell Biol **78**:249–255.
32. Ory S, Munari-Silem Y, Fort P, Jurdic P 2000 Rho and Rac exert antagonistic functions on spreading of macrophage-derived multinucleated cells and are not required for actin fiber formation. J Cell Sci **113**:1177–1188.
33. Faccio R, Novack DV, Zallone A, Ross FP, Teitelbaum SL 2003 Dynamic changes in the osteoclast cytoskeleton in response to growth factors and cell attachment are controlled by beta3 integrin. J Cell Biol **162**:499–509.
34. Sugatani T, Hruska KA 2004 Akt1/Akt2 and mTOR/Bim play critical roles in osteoclast differentiation and survival, respectively, while Akt is dispensable for cell survival in isolated osteoclast precursors. J Biol Chem **280**:3583–3589.
35. Glantschnig H, Fisher JE, Wesolowski G, Rodan GA, Reszka AA 2003 M-CSF, TNFalpha and RANK ligand promote osteoclast survival by signaling through mTOR/S6 kinase. Cell Death Differ **10**:1165–1177.
36. Yang FC, Kapur R, King AJ, Tao W, Kim C, Borneo J, Breese R, Marshall M, Dinauer MC, Williams DA 2000 Rac2 stimulates Akt activation affecting BAD/Bcl-XL expression while mediating survival and actin function in primary mast cells. Immunity **12**:557–568.
37. Genot EM, Arrieumerlou C, Ku G, Burgering BM, Weiss A, Kramer IM 2000 The T-cell receptor regulates Akt (protein kinase B) via a pathway involving Rac1 and phosphatidylinositide 3-kinase. Mol Cell Biol **20**:5469–5478.
38. Reif K, Nobes CD, Thomas G, Hall A, Cantrell DA 1996 Phosphatidylinositol 3-kinase signals activate a selective subset of Rac/Rho-dependent effector pathways. Curr Biol **6**:1445–1455.
39. Han J, Luby-Phelps K, Das B, Shu X, Xia Y, Mosteller RD, Krishna UM, Falck JR, White MA, Broek D 1998 Role of substrates and products of PI 3-kinase in regulating activation of Rac-related guanosine triphosphatases by Vav. Science **279**:558–560.
40. Welch HC, Coadwell WJ, Stephens LR, Hawkins PT 2003 Phosphoinositide 3-kinase-dependent activation of Rac. FEBS Lett **546**:93–97.

Address reprint requests to:
Sakae Tanaka, MD, PhD
7-3-1 Hongo, Bunkyo-ku
Tokyo 113-0033, Japan
E-mail: tanakas-ort@h.u-tokyo.ac.jp

Received in original form February 4, 2005; revised form August 1, 2005; accepted August 15, 2005.

THE JOURNAL OF BIOLOGICAL CHEMISTRY VOL. 280, NO. 50, pp. 41700–41706, December 16, 2005

Identification of an Alternatively Spliced Variant of Ca^{2+}-promoted Ras Inactivator as a Possible Regulator of RANKL Shedding*

Received for publication, June 27, 2005, and in revised form, October 16, 2005 Published, JBC Papers in Press, October 18, 2005, DOI 10.1074/jbc.M507000200

Atsuhiko Hikita[‡], Yuho Kadono[‡], Hirotaka Chikuda[‡], Akira Fukuda[‡], Hidetoshi Wakeyama[‡], Hisataka Yasuda[§], Kozo Nakamura[‡], Hiromi Oda[¶], Tsuyoshi Miyazaki[‡], and Sakae Tanaka[‡‖]

From the [‡]Department of Orthopaedic Surgery, Faculty of Medicine, The University of Tokyo, 7-3-1 Hongo, Bunkyo-ku, Tokyo 113-0033, Japan, the [§]Center for Experimental Medicine, Institute of Medical Science, The University of Tokyo, 4-6-1 Shirokanedai, Minato-ku, Tokyo 108-8639, Japan, and the [¶]Department of Orthopaedic Surgery, Saitama Medical School, 38 Morohongo, Moroyama-machi, Iruma-gun, Saitama 350-0495, Japan

The receptor activator of NF-κB ligand (RANKL), a critical regulator of osteoclastogenesis, is synthesized as a membrane-anchored protein and cleaved into a soluble form by ectodomain shedding. We developed an assay system to identify molecules regulating the RANKL shedding. Using this system, we found that a splice variant of Ca^{2+}-promoted Ras inactivator (CAPRI), ΔCAPRI, which is expressed in primary osteoblasts, promoted the RANKL shedding. The wild type CAPRI is a member of the Ras GTPase-activating protein (GAP) family and suppresses Ca^{2+}-dependent Ras activation, whereas ΔCAPRI, which lacks one exon in the GAP-related domain, activated the Ras pathway. Overexpression of ΔCAPRI or a constitutive active form of Ras up-regulated the expression level of matrix-metalloproteinase 14 (MMP14), which directly cleaves the ectodomain of RANKL, whereas Erk activation by expressing the constitutive active Mek1 did not affect the MMP14 expression or RANKL shedding. These results suggest that ΔCAPRI is a possible regulator of RANKL shedding by modulating MMP14 expression through Ras signaling cascades other than the Erk pathway.

The receptor activator of NF-κB ligand, RANKL (also known as TNF-related activation-induced cytokine, TRANCE, osteoprotegrin ligand, OPGL, and osteoclast differentiation factor, ODF) is a type II transmembrane glycoprotein with a molecular mass of ~45 kDa, which belongs to the tumor necrosis factor (TNF)[2] ligand family (1–5). RANKL is expressed on the membrane of osteoblasts and bone marrow stromal cells and binds to and activates TNF family receptor RANK expressed on monocyte-macrophage lineage osteoclast precursors (3, 4). Upon binding to RANKL, RANK activates the intracellular signaling pathways including NF-κB, Erk, JNK, and NFATc1, and leads to osteoclast differentiation, activation, and survival (6, 7). The essential role of RANKL in normal bone turnover was further established by a series of knock-out mice, *i.e.* both RANKL- and RANK-deficient animals exhibited severe osteopetrosis because of the lack of osteoclast differentiation (8, 9), whereas the targeted disruption of osteoprotegerin, a natural inhibitor of RANKL, developed severe osteoporosis because of enhanced osteoclastogenesis (10).

Some transmembrane proteins are extracellularly cleaved and released into the surrounding environment. RANKL is also made as a membrane-bound protein, cleaved by some proteinases, and converted to the soluble RANKL (11, 12). This process, known as ectodomain shedding, has a diverse effect on a wide variety of membrane-bound proteins. For example, when TNF-α is cleaved by the TNF-α converting enzyme and released into the circulatory system, it exhibits strong systemic effects (13, 14). In contrast, the Fas ligand is a strong apoptosis inducer in its membrane-bound form, but the soluble Fas ligand has fewer effects on apoptosis induction (15).

Although some proteinases have been demonstrated to have the RANKL shedding activity, no definite RANKL sheddase(s) have yet been identified. TNF-α converting enzyme was reported to be a candidate of RANKL sheddase (11); however, a more recent study has shown that TNF-α converting enzyme had no apparent effect on the RANKL shedding and that the RANKL shedding in TNF-α converting enzyme-deficient cells was indistinguishable (16). A disintegrin and metalloproteinase domain family (ADAM)19 has also been reported to exhibit RANKL shedding activity (17), but embryonic fibroblasts from ADAM19 knock-out mice showed almost the same RANKL shedding activity as the cells from the wild type animals (16). Matrix metalloproteinase 14 (MMP14, also called the membrane-type 1 matrix metalloproteinase, MT1-MMP) can also cleave RANKL, although its cleavage site differs from that previously reported (16). These results suggest that there are other molecules implicated in RANKL shedding.

To identify molecules involved in the regulation of RANKL shedding, we developed a novel screening system, in which expression plasmids encoding secreted placental alkaline phosphatase (SEAP) fused with mouse C-terminally truncated RANKL (tRANKL-SEAP) were co-transfected with cDNA library pools of ST2 cells. Utilizing this screening system, we found that an alternatively spliced variant of Ca^{2+}-promoted Ras inactivator (CAPRI), ΔCAPRI led to an increase in the RANKL shedding.

MATERIALS AND METHODS

Reagents—*p*-Nitrophenyl phosphate was purchased from Sigma-Aldrich. DNA polymerase, Pyrobest (for subcloning), was purchased from Takara biochemicals (Shiga, Japan), KOD plus (for reverse transcription-PCR) was from Toyobo (Osaka, Japan), and ionomycin was from Merck. Antibodies were purchased as follows: for the His tag, Erk, phosphorylated Erk, integrin-β and HSP-90 from Santa Cruz Biotechnology,

* This work was supported by grants-in-aid from the Ministry of Education, Culture, Sports, Science and Technology of Japan and the Health Science research grants from the Ministry of Health, Labour and Welfare of Japan (to S. T.). The costs of publication of this article were defrayed in part by the payment of page charges. This article must therefore be hereby marked "*advertisement*" in accordance with 18 U.S.C. Section 1734 solely to indicate this fact.

‖ To whom correspondence should be addressed. Tel.: 81-3-3815-5415 (ext. 33376); Fax: 81-3-3818-4082; E-mail: TANAKAS-ORT@h.u-tokyo.ac.jp.

[2] The abbreviations used are: TNF, tumor necrosis factor; Erk, extracellular signal-regulated kinase; JNK, c-Jun NH_2-terminal kinase; CAPRI, Ca^{2+}-promoted Ras inactivator; GAP, GTPase-activating protein; MMP14, matrix metalloproteinase 14; SEAP, secreted placental alkaline phosphatase; wt, wild type; Mek, mitogen-activated protein kinase/extracellular signal-regulated kinase kinase.

Inc. (Santa Cruz, CA), for the V5 tag from Invitrogen, for actin from Sigma-Aldrich, and for RANKL from Active Motif (Carlsbad, CA).

Division of ST2 cDNA Library and Plasmid Purification—Procedures for the construction of the ST2 cDNA library were previously described (3). Competent high DH5α (Toyobo) *Escherichia coli* cells were transformed by heat shock with DNA solution of the ST2 cDNA library, and the library was divided into 1000 subpools, each of which contained ~100 clones. After the first screening was completed, every positive pool was divided into 48 subpools each of which contained ~10 clones and was subjected to a second screening, and the resulting positive pools were divided into 48 single clones. The plasmids were purified from *E. coli* using the QIAprep Spin Miniprep Kit (Qiagen, Hilden, Germany).

Constructs—The expression vectors for the mutants of Ras, pcDNA3-RasV12 (a constitutively active mutant) and pcDNA3-RasN17 (a dominant negative mutant), were generous gifts from Dr. C. Kitanaka (Yamagata University). An expression vector for a constitutively active form of Mek1, pcDNA3.1(+)-Mek^{CA}, was constructed by insertion of the cDNA fragments digested from pGEM-Mek^{CA} (generous gift from K. Arai, Research Institute, National Rehabilitation Center for Persons with Disabilities) to NotI restriction site of pcDNA3.1(+) (Invitrogen). The tRANKL-SEAP expression vector was constructed as follows. The cDNA encoding for SEAP was subcloned from pSEAP2-Control (Clontech) by PCR using a set of primers, 5′-CGCTCGAGAATCATCCCAGTTGAGGAGGAGA-ACC-3′ and 5′-GCGTCTAGAGTAACCCGGGTGCGCGG-3′, and the cDNA fragment of the cytoplasmic region, transmembrane domain, and stalk region of the mouse RANKL (corresponding to amino acids 4–157) were subcloned from ST2 cDNA library by PCR using a set of the following primers: 5′-AAGCTTGCCACCATGGCCAGCCGAGACTACGGCA-A-3′ and 5′-GCGGCCGCCGCCTCGCTGGGCCACATCCA-3′. The PCR fragments were ligated into pCR-blunt II TOPO (Invitrogen) using protocols recommended by the manufacturer. The SEAP fragment and the RANKL fragment were digested from TOPO vectors with XhoI/XbaI and HindIII/NotI, respectively, and inserted into the corresponding restriction sites of pcDNA3.1-V5HisA (Invitrogen). The full-length RANKL was cloned from the cDNA of primary osteoblasts by PCR and inserted into the HindIII/NotI sites of pcDNA3.1-V5HisB (Invitrogen). The wild type CAPRI was cloned from the cDNA of primary osteoblasts, and ΔCAPRI was subcloned from pcDL-ΔCAPRI by PCR (for pcDL-SRα vector, see Ref. 18) and inserted into the EcoRI/NotI sites of pEF1-HisC (Invitrogen) and the EcoRI/XhoI sites of pcDNA3.1-V5HisA (Invitrogen). The cDNA for full-length MMP14 was digested from pcDL-MMP14 at SalI sites and inserted into XhoI sites of pcDNA3.1(+). The cDNA for MMP13 was cloned from the cDNA of primary osteoblasts by PCR, and inserted into the HindIII/XbaI sites of pcDNA3.1-V5HisA. Small interfering RNA plasmids for MMP14 were constructed using piGENE U6 vector (iGENE Therapeutics Inc., Ibaraki, Japan) according to manufacturer's protocol. The target sites were 5′-GGGCTGAGATCAAGGCCAA-TG-3′ and 5′-GCGGGTGAGGAATAACCAAGT-3′.

Cell Culture and Transfection—The human kidney cell line 293T, human osteosarcoma cell line SaOS2, and mouse fibroblast cell line NIH3T3 were cultured with Dulbecco's modified Eagle's medium (Sigma) supplemented with 10% fetal bovine serum and 1% penicillin-streptomycin solution (Sigma) at 37 °C in a humidified atmosphere containing 5% CO_2. The plasmids were transfected into the cells using the FuGENE 6 transfection reagent (Roche Diagnostics) according to the manufacturer's instructions.

Alkaline Phosphatase Assay of Culture Medium—293T cells were seeded in 96-well cell culture plates at a concentration of 5×10^5 cells/ml. 24 h later, 625 pg of pcDNA3.1-tRANKL-SEAP and 49.375 ng of a subpool of the ST2 cDNA library or other constructs were co-transfected to 293T using FuGENE 6. 72 h after the transfection, 50 μl of the culture medium was collected from each well and subjected to an alkaline phosphatase assay. In brief, the culture medium was incubated with 125 μl of dH_2O, 100 mM $NaHCO_3$, 100 mM Na_2CO_3, 1 mM $MgCl_2$, and 2 mM *p*-nitrophenyl phosphate at 65 °C for 90 min, and then the absorbance of the solution at a wavelength of 405 nm was measured using the MTP-300 microplate reader (CORONA Electric, Ibaraki, Japan).

DNA Sequencing of Positive Clones—DNA sequences of the positive clones were determined by the cycle sequencing method. In brief, samples were prepared using the BigDye terminator Ver 1.0 (Applied Biosystems, Foster City, CA) and DyeEx 2.0 spin kit (Qiagen) and then analyzed using the ABI PRISM® 310 Genetic Analyzer (Applied Biosystems).

Reverse Transcription-PCR—The procedures for preparation of the primary osteoblasts from the calvaria of newborn C57/BL6 mice and for formation of osteoclasts were previously described (19, 20). The total RNA was purified from primary osteoblasts and osteoclasts using ISOGEN (Nippon Gene Co. Ltd., Toyama, Japan) according to the method recommended by the manufacturer. The cDNA was synthesized from purified RNA using SuperScript II reverse transcriptase (Invitrogen). The primers used for the PCR analysis of ΔCAPRI were 5′-GGCTGGC-CAAGGACTTTCTG-3′ and 5′-CTATGTTCTGGACCGCCTGG-3′.

Western Blotting—The procedure for Western blotting was described previously (20). To detect the soluble RANKL released into the supernatants, 3 ml of the culture medium were incubated with 6 μl of recombinant protein G-agarose (Invitrogen) and 1 μg of recombinant osteoprotegerin-Fc chimeric protein (R&D Biosystems) for 16 h at 4 °C, then recovered by brief centrifugation. The pellets were suspended in TNE buffer (10 mM Tris-HCl (pH 7.5), 150 mM NaCl, 1 mM EDTA, 1% Nonidet P-40) and subjected to SDS-PAGE. Membrane fraction was gained using Mem-PER mammalian protein extraction reagent (Pierce Chemical Co.).

Immunocytochemistry—NIH3T3 cells were transfected with pcDNA3.1-ΔCAPRI-V5HisA or -wtCAPRI and, 24 h later, were unstimulated or stimulated with 5 μg/ml ionomycin for 2 min. The cells were then fixed with 4% paraformaldehyde, permeabilized with 0.2% Triton-X, and immunostained with anti-V5 antibody and Alexa Fluor® 488 goat anti-mouse IgG (Molecular probes, Eugene, OR).

Real Time PCR—The reaction mixture for the real time PCR was prepared using qPCR QuickGoldStar Mastermix Plus for SYBR® Green I (Nippon Gene, Tokyo, Japan) and was analyzed using the Mx3000P™ QPCR System (Stratagene, La Jolla, CA). The set of primers used were 5′-GCTCACCCCAGTCACTCTCA-3′ and 5′-CTCATGGCCTTC-ATGGTGTC-3′ for MMP14 and 5′-GAAGGTGAAGGTCGGAGT-CA-3′ and 5′-GAAGATGGTGATGGGATTTC-3′ for glyceraldehyde-3-phosphate dehydrogenase.

Statistical Analysis—A statistical analysis was performed using the Student's *t* test for alkaline phosphatase assay and the unpaired Student's *t* test for real time PCR.

RESULTS

Development of a Screening System for Molecules with RANKL Shedding Activity—To identify molecules potentially involved in the regulation of RANKL shedding, we developed a new library screening system. We constructed an expression vector encoding the fusion protein of SEAP with the C-terminally truncated form of RANKL, which contains the stalk region, transmembrane domain, and intracellular domain of RANKL (tRANKL-SEAP) (Fig. 1*A*). Clear up-regulation of the alkaline phosphatase activity was detected in the culture medium when this

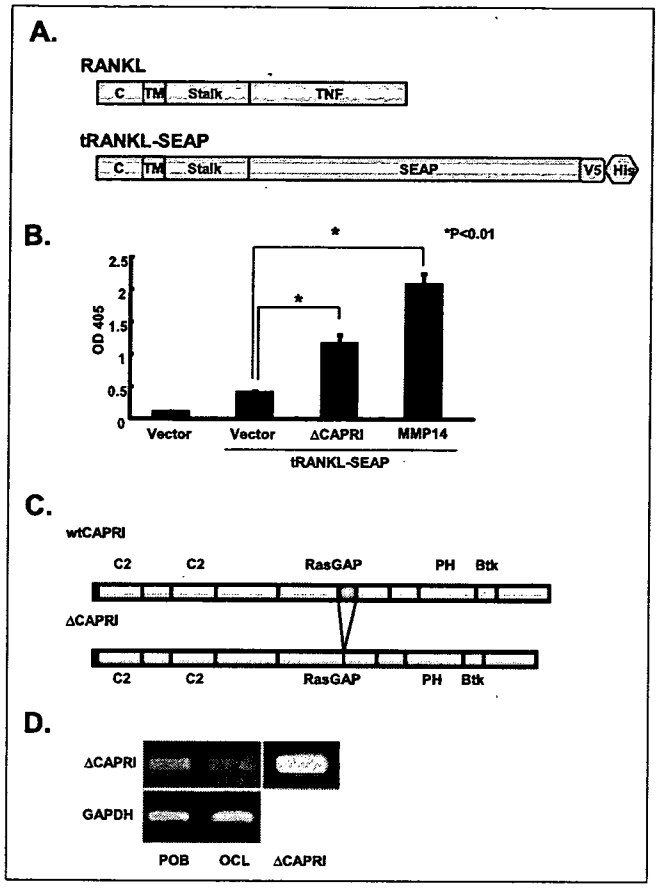

FIGURE 1. **Identification of ΔCAPRI as a possible regulator of RANKL shedding.** *A*, schematic representation of RANKL and the tRANKL-SEAP fusion protein. tRANKL-SEAP is a fusion protein of SEAP with C-terminally truncated RANKL, which contains the stalk region but lacks the TNF-like domain of RANKL, and with V5 and His_6 tags at the C terminus. *C*, cytoplasmic domain; *TM*, transmembrane domain; *Stalk*, stalk region; *TNF*, TNF-like domain. *B*, alkaline phosphatase activity of the culture medium of 293T cells transfected with pcDNA3.1-tRANKL-SEAP and pcDL-SRα, pcDL-ΔCAPRI or pcDL-MMP14. *, significantly different, $p < 0.01$ *C*, schematic representation of an alternative splice variant of CAPRI (ΔCAPRI), which lacks part of the RasGAP domain. *PH*, pleckstrin homology domain; *Btk*, Bruton's tyrosine kinase motif. *D*, expression of ΔCAPRI in primary osteoblasts. Reverse transcription-PCR with specific primers for ΔCAPRI showed clear expression of ΔCAPRI in primary osteoblasts (*left lane*), but low expression in osteoclasts (*middle lane*). The *right lane* shows the positive control of ΔCAPRI using pcDNA3.1-ΔCAPRI plasmids as templates. *POB*, primary osteoblast; *OCL*, osteoclast.

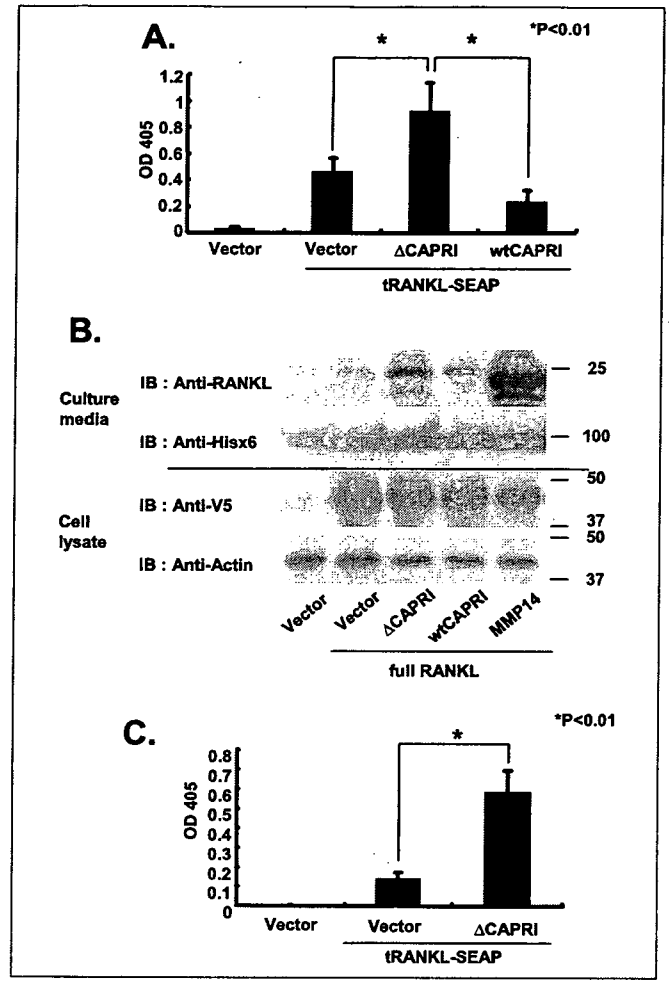

FIGURE 2. **ΔCAPRI expression promotes RANKL shedding.** *A*, alkaline phosphatase activity in the culture supernatants of 293T cells co-transfected with pcDNA3.1-tRANKL-SEAP and pEF1-His, pEF1-ΔCAPRI, or pEF1-wtCAPRI. Up-regulation of alkaline phosphatase activity was observed only in the pEF1-ΔCAPRI-transfected cell supernatants. *, significantly different, $p < 0.01$ *B*, Western blot analysis of cleaved RANKL. 293T cells were co-transfected with full-length RANKL expression vector and pEF1-His, -ΔCAPRI, -wtCAPRI, or pcDNA3.1(+)-MMP14 and incubated for 72 h. Osteoprotegerin-Fc in the culture media and RANKL in the cell lysates were probed with anti-His and anti V5 antibody, respectively. *C*, ΔCAPRI expression induces RANKL shedding in osteoblastic cells. Alkaline phosphatase activity of the culture media of SaOS2 cells transfected with pcDNA3.1-tRANKL-SEAP and pcDL-SRα or pcDL-ΔCAPRI. Up-regulation of alkaline phosphatase activity in pcDL-ΔCAPRI-transfected cells was observed. *, significantly different, $p < 0.01$.

plasmid was co-transfected with the MMP14 expression vector into 293T cells (data not shown), indicating that this assay system is suitable for screening molecules with the RANKL shedding activity. Using this assay system, we screened the cDNA library of the mouse bone marrow-derived stromal cell line, ST2 cells for molecules with RANKL shedding activity. From 1×10^6 clones, 12 positive clones were isolated. Nucleotide sequences of these cDNA fragments revealed that one of the positive clones encoded a full-length cDNA for a novel splice variant of CAPRI, which lacks one exon (138 bp) in the RasGAP domain of the wild type CAPRI (ΔCAPRI) (Fig. 1, *B* and *C*). The other clones included full-length MMP14 (Fig. 1*B*), which was already reported to increase the RANKL shedding (16). The reverse transcription-PCR analysis showed that ΔCAPRI is expressed in mouse primary osteoblasts and osteoclasts (Fig. 1*D*).

ΔCAPRI Expression Increases RANKL Shedding—We next examined the effect of ΔCAPRI and wtCAPRI on the RANKL shedding. Either the ΔCAPRI or the wtCAPRI expression plasmid was transfected to the 293T cells with the tRANKL-SEAP construct, and the alkaline phosphatase activity in culture media was measured using *p*-nitrophenyl phosphate as substrate. The 293T cells co-transfected with the tRANKL-SEAP expression plasmid and empty vector exhibited a very low level of alkaline phosphatase activity in the supernatant. Similarly, a low alkaline phosphatase activity was detected in the conditioned medium of the cells expressing wtCAPRI. In contrast, the co-expression of ΔCAPRI significantly increased the amount of tRANKL-SEAP released into the supernatant, suggesting that the ΔCAPRI expression induces the cleavage of membrane-anchored RANKL in transfected 293T cells (Fig. 2*A*). In addition, the co-transfection of ΔCAPRI and the full-length RANKL expression plasmids markedly promoted the release of RANKL as detected by Western blotting with the anti-RANKL antibody (Fig. 2*B*). We next examined the effect of ΔCAPRI on the RANKL shedding in osteoblastic cells. Overexpression of ΔCAPRI also promoted the RANKL shedding in the osteoblastic cell line SaOS2 cells (Fig. 2*C*).

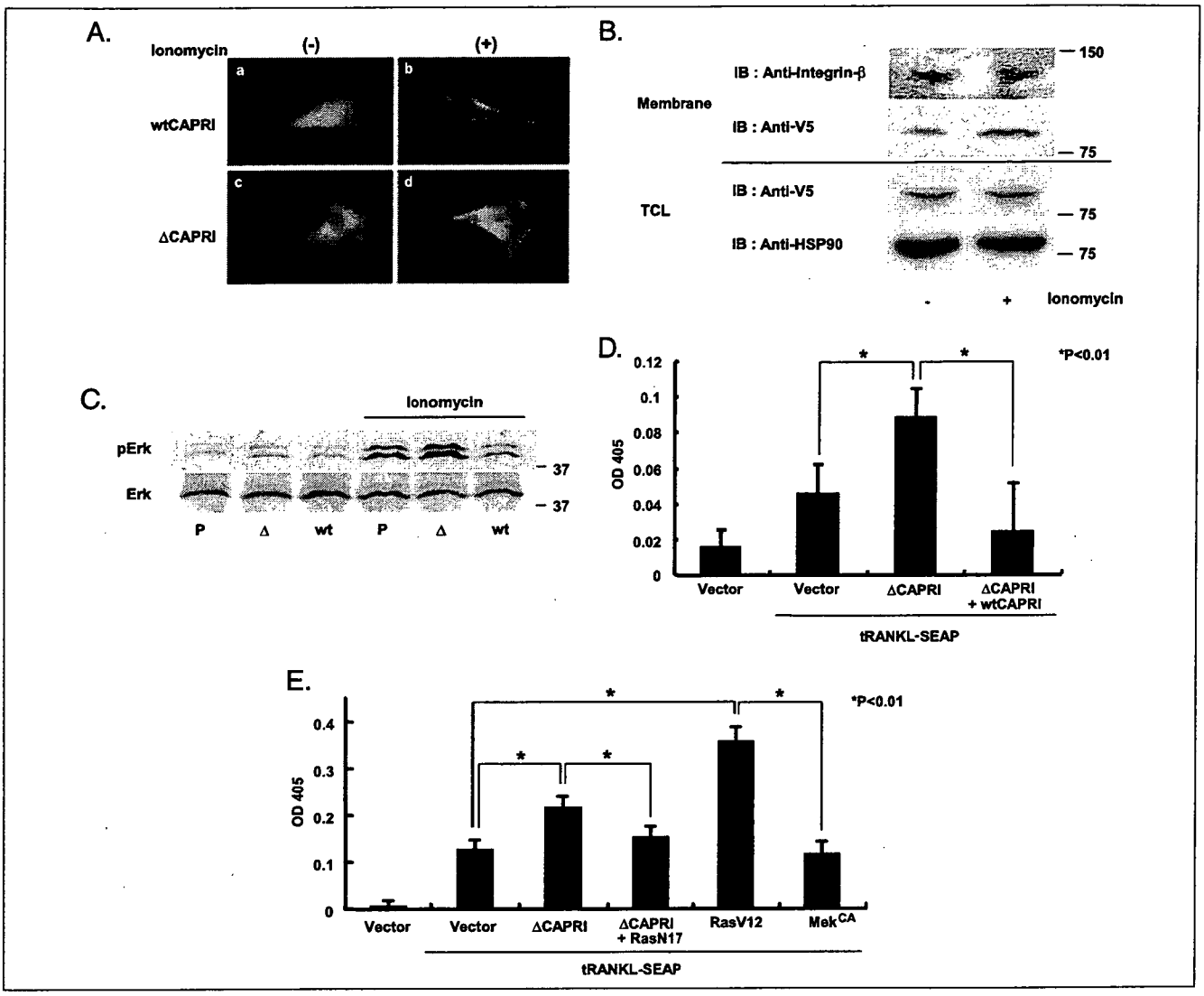

FIGURE 3. **Modulation of Ca^{2+}-induced intracellular signaling by ΔCAPRI.** *A* and *B*, translocation of wtCAPRI and ΔCAPRI to plasma membrane in response to ionomycin stimulation. *A*, NIH3T3 cells transfected with either pcDNA3.1-ΔCAPRI-V5HisA or -wtCAPRI were unstimulated (*a* and *c*) or stimulated with 5 μg/ml ionomycin for 2 min (*b* and *d*) and immunostained with anti-V5 antibody. Note the translocation of both wtCAPRI and ΔCAPRI from cytoplasm to plasma membrane upon stimulation with ionomycin. *B*, 293T cells were transfected with pcDNA3.1-ΔCAPRI-V5HisA, and 48 h later, membrane fraction and total cell lysates of cells unstimulated (*left lane*) or stimulated (*right lane*) with 5 μg/ml ionomycin for 2 min were subjected to SDS-PAGE. Integrin-β was used as a marker for the membrane fraction, and HSP90 as an internal control of total cell lysates. Ionomycin treatment up-regulated the membrane localization of ΔCAPRI as shown by the anti-V5 blotting, whereas the amount of ΔCAPRI in the total cell lysates did not appear to differ. *TCL*, total cell lysates. *C*, ΔCAPRI promotes ionomycin-induced Erk activation. 293T transfected with pcDNA3.1-V5HisA, -ΔCAPRI, or -wtCAPRI were incubated for 36 h and serum-starved for 12 h. Cells were stimulated by 5 μg/ml of ionomycin for 2 min and subjected to Western blot analysis. ΔCAPRI expression increased ionomycin-induced Erk activation, whereas wtCAPRI expression suppressed it. *P*, pcDNA3.1-V5HisA; Δ, pcDNA3.1-ΔCAPRI-V5HisA; *wt*, pcDNA3.1-wtCAPRI-V5HisA. *D* and *E*, alkaline phosphatase activity of the supernatants of the 293T cell cultures transfected with pcDNA3.1-tRANKL-SEAP and pcDNA3.1-V5HisA, -ΔCAPRI, wtCAPRI, pcDNA3-RasV12, -RasN17, or pcDNA3.1(+)-Mek^{CA}. *, significantly different, $p < 0.01$.

ΔCAPRI Activates Ras Signaling Pathways—Lockyer *et al.* (21) reported that the elevation of the intracellular Ca^{2+} causes a rapid C2 domain-dependent translocation of wtCAPRI to the plasma membrane, resulting in the activation of the RasGAP activity and the inactivation of the Ras/Mek/Erk pathways. Therefore, we investigated the translocation of wt and ΔCAPRI after the Ca^{2+} influx by the Ca^{2+} ionophore ionomycin treatment and found that both the wt and ΔCAPRI moved to the plasma membrane of NIH3T3 and 293T cells 2 min after the ionomycin stimulation as shown in Fig. 3*A* by immunocytochemistry and Fig. 3*B* by cell fractionation analysis. To investigate whether ΔCAPRI modulates the Ras/Erk signaling pathway, we examined the Erk activity in the ΔCAPRI- or wtCAPRI-overexpressing 293T cells. As shown in Fig. 3*C*, the overexpression of ΔCAPRI enhanced the ionomycin-induced Erk phosphorylation, whereas the wtCAPRI expression reduced the Erk activation, indicating that ΔCAPRI works in a dominant negative fashion. In fact, wtCAPRI suppressed RANKL shedding promoted by ΔCAPRI (Fig. 3*D*).

Ras Activation, but Not Mek/Erk Pathway, Is Involved in RANKL Shedding—Because CAPRI is a Ca^{2+}-sensitive RasGAP, we next tested whether the Ras activity is involved in the RANKL shedding. As shown in Fig. 3*E*, the expression of the constitutively active Ras strongly promoted the RANKL shedding in the 293T cells. RANKL shedding induced by the ΔCAPRI overexpression was significantly suppressed by the co-expression of a dominant negative mutant of Ras (RasN17). These results indicate that the Ras activity plays an important role in the regulation of the RANKL shedding induced by ΔCAPRI. Interestingly, however, the up-regulation of Erk activity in the 293T cells with the constitutively active Mek1 expression (Mek^{CA}) did not increase the alkaline phosphatase activity released into the supernatant (Fig. 3*E*).

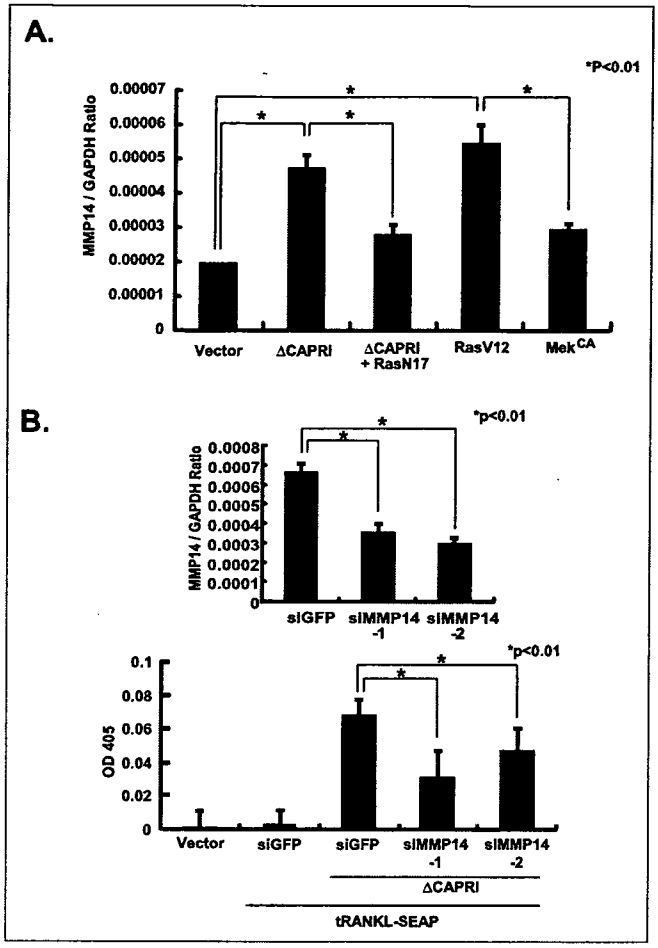

FIGURE 4. **ΔCAPRI-Ras-MMP14 axis plays an important role in the RANKL shedding.** *A*, ΔCAPRI and Ras^{CA} increases the expression of MMP14. mRNA level of MMP14 in 293T cells measured by real time PCR. 293T cells were transfected with pcDNA3.1-V5HisA, -ΔCAPRI, pcDNA3-RasV12, -RasN17, or pcDNA3.1(+)-Mek^{CA}. Forty-eight hours later, RNA was extracted and subjected to real time PCR. *, significantly different, $p < 0.01$ *B*, MMP14 knockdown suppresses RANKL shedding. SaOS2 cells were transfected with pU6-siGFP, -siMMP14-1, or -2, and MMP14 expression was analyzed by real time PCR (*upper panel*). MMP14 knockdown using these constructs suppressed ΔCAPRI-induced RANKL shedding as shown by alkaline phosphatase activity in the culture media (*lower panel*).

Ras Activity Regulates the Expression Level of MMP14—ST2 cDNA library screening for the RANKL shedding confirmed that MMP14 could be a candidate for the RANKL sheddase, and in fact, the co-transfection of MMP14 expression vector with pcDNA3.1-tRANKL-SEAP significantly increased the amount of tRANKL-SEAP released into the supernatant (Fig. 1*B*). We next examined whether or not the Ras activation downstream of ΔCAPRI is involved in the expression level of MMP14. In the real time PCR analysis from mRNA of the 293T cells, ΔCAPRI up-regulated MMP14, which was significantly suppressed by the co-expression of Ras^{DN}. Ras^{CA} induced the up-regulation of MMP14, whereas Mek^{CA} did not affect the expression level of MMP14 (Fig. 4*A*). This result suggested that ΔCAPRI would promote the RANKL shedding through up-regulation of MMP14. To confirm this, we constructed siRNA vectors for MMP14. As shown in Fig. 4*B*, siMMP14-1 and -2 suppressed expression of endogenous MMP14 in SaOS2 cells (*upper panel*), and the RANKL shedding promoted by ΔCAPRI (*lower panel*).

MMP14 Has Much Stronger RANKL Shedding Activity than MMP13—Inada *et al.* (22) recently reported that MMP13-deficient mice had skeletal abnormalities such as increased trabecular bone mass.

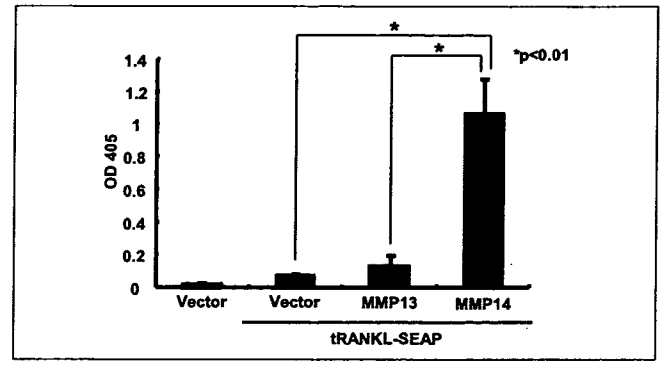

FIGURE 5. **MMP13 has much weaker effect on RANKL shedding compared with MMP14.** Alkaline phosphatase activity of the culture medium of 293T cells transfected with pcDNA3.1-tRANKL-SEAP and pcDNA3.1-V5HisA, -MMP13, or -MMP14. *, significantly different, $p < 0.01$.

To examine the relevance of this proteinase in RANKL shedding, we transfected the MMP13 expression vector and tRANKL-SEAP to 293T cells. Overexpression of MMP13 exhibited little effect on the up-regulation of the alkaline phosphatase activity in the supernatant, indicating that MMP13 had much weaker RANKL shedding activity compared with MMP14 (Fig. 5).

DISCUSSION

Ectodomain shedding is a highly regulated process that affects a number of transmembrane proteins, and is considered to play an important role in regulating various pathophysiological events. The role of ectodomain shedding varies between substrate proteins. For example, shedding allows some local growth factors, such as TNF-α and epidermal growth factor, to be released from the local environments and participate in the paracrine and endocrine signalings (13, 14, 23). Interestingly, proteolytic processing via shedding is important even for the local effects of the growth factors such as epidermal growth factor (24).

RANKL is a key molecule for the osteoclastogenesis and bone-resorbing activity of mature osteoclasts. RANKL is produced as a membrane-bound cytokine and released into the paracrine and the endocrine milieu via ectodomain shedding, although the biological significance of RANKL shedding is still unknown. The soluble form of RANKL induces *in vitro* osteoclastogenesis from bone marrow cells, and several studies have revealed an increase in the intraarticular level of soluble RANKL under pathological conditions such as rheumatoid arthritis (25). Recently, Mizuno *et al.* (26) generated transgenic animals overexpressing soluble RANKL in the liver after birth that exhibited a marked decrease in bone mineral density with aging, indicating that the excessive production of soluble RANKL can promote *in vivo* osteoclastogenesis. On the other hand, it was reported that the membrane-bound RANKL is more potent in stimulating osteoclast differentiation than its soluble form (12). To reveal the biological and pathological relevance of RANKL shedding, elucidating the molecular mechanism underlying RANKL shedding is indispensable.

It is difficult to detect soluble RANKL in the culture medium by the usual Western blot analysis because the expression level of RANKL is relatively low. Nakashima *et al.* (12) developed a ligand-receptor precipitation Western blot analysis using osteoprotegerin, which specifically binds to RANKL, but this system is not suitable for systematic screening of a large number of molecules. Blobel and coworkers (27) reported a simple and quantitative assay for TNF-α shedding using alkaline phosphatase-tagged TNF-α. This method allows the rapid and reproducible quantitation of the TNF-α shedding. We first constructed an expression vector that encodes a fusion protein of mouse full-length RANKL and

SEAP (full RANKL-SEAP) and transfected it into 293T cells. Although we could find the expression of the full RANKL-SEAP by Western blotting, we failed to detect alkaline phosphatase activity in the supernatants even when the vector was co-transfected with a putative RANKL sheddase, MMP14, the reason of which remains unclear (data not shown). For several type II transmembrane proteins including TNF-α, the juxtamembrane sequence surrounding the cleavage site has been shown to be sufficient to target the protein for regulated shedding (16). Therefore, we next constructed an expression vector encoding a fusion protein of SEAP with the C-terminally truncated RANKL, which contained the stalk region but lacked the TNF-like domain of RANKL (pcDNA3.1-tRANKL-SEAP), and transfected it together with the ST2 cell-derived cDNA library. Using this assay system, we could isolate 12 independent positive clones, which showed alkaline phosphatase activity in the supernatant when transfected with pcDNA3.1-tRANKL-SEAP. They could also increase the amount of soluble RANKL when transfected into the 293T cells with the full-length RANKL, confirming the relevance of this screening system.

One of the positive clones was a spliced variant of CAPRI. The protease activity inducing ectodomain shedding of the transmembrane proteins has been reported to be modulated by protein kinase signaling such as the Ras/Mek/Erk pathway (28). CAPRI was originally identified as a member of the RasGAP, negative regulators of Ras signaling pathways (21, 29), and the R473S mutation decreased the RasGAP activity of CAPRI and enhanced ATP- or ionomycin-induced Erk phosphorylation (21). ΔCAPRI lacks the Arg-473-containing exon in the RasGAP domain in which the FLR motif stabilizes the catalytic arginine-finger loop (30), suggesting that it can work in a dominant negative fashion like the R473S mutant, and in fact, the ΔCAPRI expression increased the ionomycin-induced Erk activation, and co-expression of wtCAPRI diminished the RANKL shedding promoted by ΔCAPRI. The expression of a dominant negative mutant of Ras (RasN17) suppressed the RANKL shedding induced by ΔCAPRI, and a constitutively active mutant of Ras (RasV12) expression stimulated the RANKL shedding, indicating that ΔCAPRI induces RANKL shedding via activating Ras pathways.

The only protease we could isolate in this screening system was MMP14 (MT1-MMP), which was previously reported as a candidate of the RANKL sheddases (16). It should be noticed that MMP14 knock out mice showed an increase in osteoclast number and developed severe osteopenia (31). This suggests that MMP14 negatively regulates the local osteoclastogenesis by reducing membrane-bound RANKL through ectodomain shedding, although it may increase the amount of soluble RANKL. The serum concentration of soluble RANKL in the physiological condition is reportedly less than 1 ng/ml, which is not high enough to induce general osteopenia (32).

Our data do not exclude the possibility that other proteases than MMP14 are involved in this process. Recent studies have demonstrated the role of MMP13 in regulating bone integrity; however, RANKL shedding activity of MMP13 was much weaker than that of MMP14. The overexpression of ΔCAPRI or Ras^{CA} increased the expression of MMP14, and MMP14 knockdown suppressed RANKL shedding promoted by ΔCAPRI, indicating that the ΔCAPRI/Ras pathways stimulate the RANKL shedding by regulating the expression of MMP14.

Interestingly, the constitutively active Mek expression failed to up-regulate the amount of the cleaved RANKL or MMP14 expression, although the Erk activity was strongly up-regulated (data not shown). These results suggest that the downstream cascades of Ras other than the Mek/Erk pathway are implicated in the RANKL shedding. A further investigation is required to clarify the signal transduction pathway(s) downstream of Ras that regulates the RANKL shedding.

In conclusion, we established a novel library screening system for identifying the molecules involved in the RANKL shedding and identified a splice variant of CAPRI, ΔCAPRI, as a possible candidate. ΔCAPRI activates the Ras pathways, which increase the expression of MMP14 in a Mek/Erk-independent manner and lead to the RANKL shedding. These data suggest that the ΔCAPRI-Ras-MMP14 axis plays an important role in the RANKL shedding.

Acknowledgments—We thank R. Yamaguchi (Department of Orthopaedic Surgery, The University of Tokyo), who provided expert technical assistance, C. Kitanaka (Yamagata University) for the pcDNA3-RasV12 and -RasN17 constructs, and K. Arai (Research Institute, National Rehabilitation Center for Persons with Disabilities) for pGEM-Mek^{CA}.

REFERENCES

1. Anderson, D. M., Maraskovsky, E., Billingsley, W. L., Dougall, W. C., Tometsko, M. E., Roux, E. R., Teepe, M. C., DuBose, R. F., Cosman, D., and Galibert, L. (1997) *Nature* **390**, 175–179
2. Wong, B. R., Rho, J., Arron, J., Robinson, E., Orlinick, J., Chao, M., Kalachikov, S., Cayani, E., Bartlett, F. S., III, Frankel, W. N., Lee, S. Y., and Choi, Y. (1997) *J. Biol. Chem.* **272**, 25190–25194
3. Yasuda, H., Shima, N., Nakagawa, N., Yamaguchi, K., Kinosaki, M., Mochizuki, S., Tomoyasu, A., Yano, K., Goto, M., Murakami, A., Tsuda, E., Morinaga, T., Higashio, K., Udagawa, N., Takahashi, N., and Suda, T. (1998) *Proc. Natl. Acad. Sci. U. S. A.* **95**, 3597–3602
4. Lacey, D. L., Timms, E., Tan, H. L., Kelley, M. J., Dunstan, C. R., Burgess, T., Elliott, R., Colombero, A., Elliott, G., Scully, S., Hsu, H., Sullivan, J., Hawkins, N., Davy, E., Capparelli, C., Eli, A., Qian, Y. X., Kaufman, S., Sarosi, I., Shalhoub, V., Senaldi, G., Guo, J., Delaney, J., and Boyle, W. J. (1998) *Cell* **93**, 165–176
5. Kong, Y. Y., Feige, U., Sarosi, I., Bolon, B., Tafuri, A., Morony, S., Capparelli, C., Li, J., Elliott, R., McCabe, S., Wong, T., Campagnuolo, G., Moran, E., Bogoch, E. R., Van, G., Nguyen, L. T., Ohashi, P. S., Lacey, D. L., Fish, E., Boyle, W. J., and Penninger, J. M. (1999) *Nature* **402**, 304–309
6. Wong, B. R., Josien, R., Lee, S. Y., Vologodskaia, M., Steinman, R. M., and Choi, Y. (1998) *J. Biol. Chem.* **273**, 28355–28359
7. Takayanagi, H., Kim, S., Koga, T., Nishina, H., Isshiki, M., Yoshida, H., Saiura, A., Isobe, M., Yokochi, T., Inoue, J., Wagner, E. F., Mak, T. W., Kodama, T., and Taniguchi, T. (2002) *Dev. Cell* **3**, 889–901
8. Kong, Y. Y., Yoshida, H., Sarosi, I., Tan, H. L., Timms, E., Capparelli, C., Morony, S., Oliveira-dos-Santos, A. J., Van, G., Itie, A., Khoo, W., Wakeham, A., Dunstan, C. R., Lacey, D. L., Mak, T. W., Boyle, W. J., and Penninger, J. M. (1999) *Nature* **397**, 315–323
9. Dougall, W. C., Glaccum, M., Charrier, K., Rohrbach, K., Brasel, K., De Smedt, T., Daro, E., Smith, J., Tometsko, M. E., Maliszewski, C. R., Armstrong, A., Shen, V., Bain, S., Cosman, D., Anderson, D., Morrissey, P. J., Peschon, J. J., and Schuh, J. (1999) *Genes Dev.* **13**, 2412–2424
10. Bucay, N., Sarosi, I., Dunstan, C. R., Morony, S., Tarpley, J., Capparelli, C., Scully, S., Tan, H. L., Xu, W., Lacey, D. L., Boyle, W. J., and Simonet, W. S. (1998) *Genes Dev.* **12**, 1260–1268
11. Lum, L., Wong, B. R., Josien, R., Becherer, J. D., Erdjument-Bromage, H., Schlondorff, J., Tempst, P., Choi, Y., and Blobel, C. P. (1999) *J. Biol. Chem.* **274**, 13613–13618
12. Nakashima, T., Kobayashi, Y., Yamasaki, S., Kawakami, A., Eguchi, K., Sasaki, H., and Sakai, H. (2000) *Biochem. Biophys. Res. Commun.* **275**, 768–775
13. Kriegler, M., Perez, C., DeFay, K., Albert, I., and Lu, S. D. (1988) *Cell* **53**, 45–53
14. Black, R. A., Rauch, C. T., Kozlosky, C. J., Peschon, J. J., Slack, J. L., Wolfson, M. F., Castner, B. J., Stocking, K. L., Reddy, P., Srinivasan, S., Nelson, N., Boiani, N., Schooley, K. A., Gerhart, M., Davis, R., Fitzner, J. N., Johnson, R. S., Paxton, R. J., March, C. J., and Cerretti, D. P. (1997) *Nature* **385**, 729–733
15. Schneider, P., Holler, N., Bodmer, J. L., Hahne, M., Frei, K., Fontana, A., and Tschopp, J. (1998) *J. Exp. Med.* **187**, 1205–1213
16. Schlondorff, J., Lum, L., and Blobel, C. P. (2001) *J. Biol. Chem.* **276**, 14665–14674
17. Chesneau, V., Becherer, J. D., Zheng, Y., Erdjument-Bromage, H., Tempst, P., and Blobel, C. P. (2003) *J. Biol. Chem.* **278**, 22331–22340
18. Takebe, Y., Seiki, M., Fujisawa, J., Hoy, P., Yokota, K., Arai, K., Yoshida, M., and Arai, N. (1988) *Mol. Cell. Biol.* **8**, 466–472
19. Suda, T., Jimi, E., Nakamura, I., and Takahashi, N. (1997) *Methods Enzymol.* **282**, 223–235
20. Yamamoto, A., Miyazaki, T., Kadono, Y., Takayanagi, H., Miura, T., Nishina, H., Katada, T., Wakabayashi, K., Oda, H., Nakamura, K., and Tanaka, S. (2002) *J. Bone*

Miner. Res. 17, 612–621
21. Lockyer, P. J., Kupzig, S., and Cullen, P. J. (2001) *Curr. Biol.* 15, 981–986
22. Inada, M., Wang, Y., Byrne, M. H., Rahman, M. U., Miyaura, C., Lopez-Otin, C., and Krane, S. M. (2004) *Proc. Natl. Acad. Sci. U. S. A.* 101, 17192–17197
23. Harris, R. C., Chung, E., and Coffey, R. J. (2003) *Exp. Cell Res.* 284, 2–13
24. Prenzel, N., Zwick, E., Daub, H., Leserer, M., Abraham, R., Wallasch, C., and Ullrich, A. (1999) *Nature* 402, 884–888
25. Kotake, S., Udagawa, N., Hakoda, M., Mogi, M., Yano, K., Tsuda, E., Takahashi, K., Furuya, T., Ishiyama, S., Kim, K. J., Saito, S., Nishikawa, T., Takahashi, N., Togari, A., Tomatsu, T., Suda, T., and Kamatani, N. (2001) *Arthritis Rheum.* 44, 1003–1012
26. Mizuno, A., Kanno, T., Hoshi, M., Shibata, O., Yano, K., Fujise, N., Kinosaki, M., Yamaguchi, K., Tsuda, E., Murakami, A., Yasuda, H., and Higashio, K. (2002) *J. Bone Miner. Metab.* 20, 337–344
27. Zheng, Y., Schlondorff, J., and Blobel, C. P. (2002) *J. Biol. Chem.* 277, 42463–42470
28. Fan, H., and Derynck, R. (1999) *EMBO J.* 18, 6962–6972
29. Bivona, T. G., Perez De Castro, I., Ahearn, I. M., Grana, T. M., Chiu, V. K., Lockyer, P. J., Cullen, P. J., Pellicer, A., Cox, A. D., and Philips, M. R. (2003) *Nature* 424, 694–698
30. Ahmadian, M. R., Stege, P., Scheffzek, K., and Wittinghofer, A. (1997) *Nat. Struct. Biol.* 4, 686–68931
31. Holmbeck, K., Bianco, P., Caterina, J., Yamada, S., Kromer, M., Kuznetsov, S. A., Mankani, M., Robey, P. G., Poole, A. R., Pidoux, I., Ward, J. M., and Birkedal-Hansen, H. (1999) *Cell* 99, 81–92
32. Nakamura, M., Udagawa, N., Matsuura, S., Mogi, M., Nakamura, H., Horiuchi, H., Saito, N., Hiraoka, B. Y., Kobayashi, Y., Takaoka, K., Ozawa, H., Miyazawa, H., and Takahashi, N. (2003) *Endocrinology* 144, 5441–5449

THE JOURNAL OF BIOLOGICAL CHEMISTRY VOL. 281, NO. 48, pp. 36846–36855, December 1, 2006

Negative Regulation of Osteoclastogenesis by Ectodomain Shedding of Receptor Activator of NF-κB Ligand*

Received for publication, July 13, 2006, and in revised form, September 6, 2006 Published, JBC Papers in Press, October 3, 2006, DOI 10.1074/jbc.M606656200

Atsuhiko Hikita[‡], Ikuo Yana[§], Hidetoshi Wakeyama[‡], Masaki Nakamura[‡], Yuho Kadono[‡], Yasushi Oshima[‡], Kozo Nakamura[‡], Motoharu Seiki[§], and Sakae Tanaka[‡1]

From the [‡]Department of Orthopaedic Surgery, Faculty of Medicine, The University of Tokyo, 7-3-1 Hongo, Bunkyo-ku, Tokyo 113-0033, and the [§]Center for Experimental Medicine, Institute of Medical Science, The University of Tokyo, 4-6-1 Shirokanedai, Minato-ku, Tokyo 108-8639, Japan

Receptor activator of NF-κB ligand (RANKL) is a transmembrane glycoprotein that has an essential role in the development of osteoclasts. The extracellular portion of RANKL is cleaved proteolytically to produce soluble RANKL, but definite RANKL sheddase(s) and the physiologic function of RANKL shedding have not yet been determined. In the present study, we found that matrix metalloproteinase (MMP) 14 and a disintegrin and metalloproteinase (ADAM) 10 have strong RANKL shedding activity. In Western blot analysis, soluble RANKL was detected as two different molecular weight products, and RNA interference of MMP14 and ADAM10 resulted in a reduction of both the lower and higher molecular weight products. Suppression of MMP14 in primary osteoblasts increased membrane-bound RANKL and promoted osteoclastogenesis in cocultures with macrophages. Soluble RANKL produced by osteoblasts from MMP14-deficient mice was markedly reduced, and their osteoclastogenic activity was promoted, consistent with the findings of increased osteoclastogenesis *in vivo*. RANKL shedding is an important process that down-regulates local osteoclastogenesis.

Receptor activator of NF-κB ligand (RANKL),[2] also known as TNF-related activation-induced cytokine, osteoprotegerin ligand, and osteoclast differentiation factor, is a type II transmembrane glycoprotein of the TNF ligand family. RANKL is expressed on the plasma membrane of osteoblasts, bone marrow stromal cells, and T-lymphocytes (1–5) and exerts its activity through binding to its TNF family receptor RANK, which is expressed on monocyte-macrophage lineage osteoclast precursors (3, 4, 6). Consequently, RANK activates downstream signaling pathways such as NF-κB, p38 mitogen-activated protein kinase, c-Jun N-terminal kinase, and nuclear factor of activated T cells c1 and leads to the differentiation, activation, and survival of osteoclasts (6–9). Both RANKL- and RANK-deficient mice develop severe osteopetrosis due to a lack of osteoclasts (10, 11). Conversely, a deficiency of osteoprotegerin (OPG), a natural inhibitor of RANKL, causes severe osteoporosis due to enhanced osteoclastogenesis (12). These findings suggest a crucial role for the RANKL/RANK/OPG axis in osteoclast development.

A number of transmembrane proteins undergo proteolysis and are released from the plasma membrane, a process called ectodomain shedding. The biologic and pathologic significance of ectodomain shedding varies between substrate proteins. For example, cytokines such as TNF-α and epidermal growth factor are released from local environments and exert their activity in paracrine and endocrine signaling by ectodomain shedding (13–15). In some cases, ectodomain shedding is necessary even for the local effects of growth factors such as epidermal growth factor (16). Although membrane-bound RANKL is converted to a soluble form through ectodomain shedding (17, 18) similar to other TNF family members, such as TNF-α (13, 14) and Fas ligand (19), the RANKL sheddases involved in physiologic and pathologic bone resorption, and the role of RANKL shedding is unknown. We report that RANKL shedding is regulated by matrix metalloproteinase (MMP) 14 and a disintegrin and metalloproteinase (ADAM) 10 in bone marrow stromal cells and osteoblasts. MMP14 is mainly involved in RANKL shedding in osteoblasts, and its deficiency up-regulates osteoclastogenesis by reducing RANKL shedding in the local bone milieu.

EXPERIMENTAL PROCEDURES

Reagents— DNA polymerase, KOD plus, was purchased from TOYOBO (Osaka, Japan). Antibodies for the His-tag were from Santa Cruz Biotechnology, Inc. (Santa Cruz, CA), antibodies for the V5 tag were from Invitrogen, antibodies for actin were from Sigma-Aldrich, and the antibody for RANKL was from Active Motif (Carlsbad, CA). MMP inhibitors, FR255031 and FR217840, were generous gifts from Astellas Pharma Inc. (Tokyo, Japan).

Constructs—The procedures for the construction of the tRANKL-SEAP expression vector, pcDNA3.1-RANKL-V5HisB, pcDNA3.1-mMMP14-V5HisA, pcDNA3.1-mMMP13-V5HisA, and expression vectors for human MT1, MT2, MT3, MT4, MT5, and MT6-MMP were described previously (20–26). An expression vector for mouse RANKL, pSG5-RANKL, was con-

* This work was supported in part by Grants-in-Aid from the Ministry of Education, Culture, Sports, Science, and Technology of Japan and the Health Science research grants from the Ministry of Health, Labor, and Welfare of Japan (to S. T.). The costs of publication of this article were defrayed in part by the payment of page charges. This article must therefore be hereby marked "*advertisement*" in accordance with 18 U.S.C. Section 1734 solely to indicate this fact.

[1] To whom correspondence should be addressed. Tel.: 81-3-3815-5415 (ext. 33376); Fax: 81-3-3818-4082; E-mail: TANAKAS-ORT@h.u-tokyo.ac.jp.

[2] The abbreviations used are: RANKL, receptor activator of NF-κB ligand; MMP, matrix metalloproteinase; ADAM, a disintegrin and metalloproteinase; OPG, osteoprotegerin; SEAP, secreted placental alkaline phosphatase; MT-MMP, membrane-type matrix metalloproteinase; siRNA, small interference RNA; PGE_2, prostaglandin E_2; IL-1, interleukin-1; M-CSF, macrophage colony-stimulating factor; ELISA, enzyme-linked immunosorbent assay; GFP, green fluorescent protein; TNF, tumor necrosis factor.

structed by inserting mouse RANKL cDNA into pSG5 (Stratagene, La Jolla, CA). Expression vectors for mouse MMP1, MMP2, MMP3, MMP7, MMP9, MMP11, MMP19, MMP23, MMP28, ADAM9, ADAM10, ADAM17, and ADAM19 were constructed by inserting the cDNA generated by reverse transcription-PCR of mRNA of mouse osteoblasts into pcDNA3.1-V5HisA (Invitrogen). The cDNA for ADAM10-V5His was further subcloned from pcDNA3.1- or ADAM10-V5HisA and inserted into the pSG5 vector. Small interference RNA (siRNA) plasmids for GFP, mouse ADAM10 and MMP14 were constructed using piGENE mU6 vector (iGENE Therapeutics Inc., Ibaraki, Japan) according to the manufacturer's protocol. Target sites were, for GFP, 5′-GCTACGTCCAGGAGCGCACCA-3′; for ADAM10, 5′-GGGTCTGTCATTGATGGAAGA-3′ and 5′-GCTGTGATTGCTCAGATATCC-3′; and for MMP14, 5′-GGACTGAGATCAAGGCCAATG-3′ and 5′- GGATGGACACAGAGAACTTCG-3′. The retrovirus vector for mouse MMP14 was constructed by inserting the cDNA fragment for mouse MMP14 into the BamHI and EcoRI restriction sites of pMX-puro (kindly provided by Toshio Kitamura, Institute of Medical Science, The University of Tokyo). Retrovirus vectors for siGFP, siMMP14, and siADAM10 were constructed as follows; cDNA fragments for siRNA, including the mouse U6 promoter were subcloned from piGENE constructs by PCR using M13F/R primers and ligated into pCR-blunt II TOPO (Invitrogen), digested by EcoRI, and inserted to the EcoRI restriction site of pMX-puro.

Cell Culture—The human kidney cell line 293T were cultured in Dulbecco's modified eagle medium (Sigma-Aldrich) and the mouse bone marrow stromal cell line TM8B2 (generous gift from Prof. Noda, Medical Research Institute, Tokyo Medical and Dental University) were cultured with α-MEM, and both of them were supplemented with 10% FBS and 1% penicillin-streptomycin solution (Sigma-Aldrich Co.). Cells were incubated at 37 °C in a humidified atmosphere containing 5% CO_2. Primary osteoblasts were harvested from the calvaria of newborn ddy (purchased from Sankyo Labo Service Co., Tokyo Japan) and C57/BL6 (MMP14-deficient mice and wild-type littermates) mice as previously described (27).

Screening of RANKL Sheddases—The alkaline phosphatase assay of the culture media and the Western blot analysis were described previously (20, 28). To detect soluble RANKL released into the culture media of TM8B2 cells, 3 ml of the culture media was incubated with 4 μl of recombinant protein G-agarose (Invitrogen) and 1 μg of recombinant OPG-Fc chimeric protein (R&D Biosystems, Minneapolis, MN) for 16 h at 4 °C, then recovered by brief centrifugation. The pellets were suspended in TNE buffer (10 mM Tris-HCl (pH 7.5), 150 mM NaCl, 1 mM EDTA, 1% Nonidet P-40), and subjected to SDS-PAGE.

Retrovirus Infection—The procedure for preparation of the retrovirus was described previously (29). Primary osteoblasts were incubated with the culture media containing retrovirus supplemented with 5 μg/ml polybrane (Sigma-Aldrich) for 16 h.

Real-time PCR—The reaction mixture for the real-time PCR was prepared using qPCR QuickGoldStar Mastermix Plus for SYBR® Green I (Nippon Gene, Tokyo, Japan), and analyzed using the ABI PRISM® 7000 Sequence Detection System (Applied Biosystems, Foster City, CA) according to the manufacturer's protocol. The set of primers used were 5′-CCCAAGGCAGCAACTTCA-3′ and 5′-CAATGGCAGCTGAGAGTGAC-3′ for mouse MMP14, 5′-TGGTGCTTCTGGACTGTCTG-3′ and 5′-TACCAGCCCAGCTTCTCAGT-3′ for mouse MT2-MMP, 5′-ATCATGGCCCCATTTTATCA-3′ and 5′-GCATTGGGTATCCATCCATC-3′ for mouse MT3-MMP, 5′-TTGAGCAGGAGGAGGAGAAA-3′ and 5′-GAGTCACCTTCTGCCACACA-3′ for mouse MT5-MMP, and 5′-AGATGTGGATCAGCAAGCAG-3′ and 5′-GCGCAAGTTAGGTTTTGTCA-3′ for mouse actin.

Western Blot of Primary Osteoblasts—Cells were treated with or without 10^{-8} M 1α,25-dihydroxyvitamin D_3 ($1\alpha,25(OH)_2D_3$), 10^{-6} M prostaglandin E_2 (PGE_2), and 10 ng/ml interleukin-1 (IL-1) for 72 h, and 10 ml of culture media were collected. Cell lysates were collected using M-PER® Mammalian Protein Extraction Reagent (Pierce) according to the manufacturer's protocol. Culture media and cell lysates were treated using the same procedure as for culture media of TM8B2.

Determination of Cleavage Sites of RANKL—pSG5-RANKL were transfected to TM8B2 cells. Seventy hours after transfection, 200 ml of the culture medium was collected, and soluble RANKL was recovered using an OPG-Fc column. Samples were subjected to SDS-PAGE, transferred to polyvinylidene membrane, and stained with Coomassie Brilliant Blue. The band was excised, and the N-terminal amino acid sequence was determined by Hokkaido System Science Co., Ltd. (Hokkaido, Japan).

ELISA—Primary osteoblasts were seeded in 48-well plates at a concentration of 1×10^5 cells/ml. If needed, cells were infected with retrovirus vectors as mentioned above. After 24 h of incubation, some cultures were treated with 10^{-8} M $1\alpha,25(OH)_2D_3$ and 10^{-6} M PGE_2 for 72 h. The concentration of RANKL in the culture media and cell lysates (homogenized in 200 μl of TNE buffer per well) was determined by ELISA system developed using a TRANCE DuoSet ELISA development kit (R&D Biosystems).

Coculture of Primary Osteoblasts and Bone Marrow Macrophages—Bone marrow macrophages were obtained from tibias of 5–8 weeks-old C57/BL6 mice by flushing the bone marrow with α-MEM, and cultured in α-MEM supplemented with 10% FBS, 1% penicillin-streptomycin solution, and 10 ng/ml M-CSF (Wako Pure Chemicals, Osaka, Japan) for 16 h, and non-adherent cells were collected. For the coculture, primary osteoblasts were seeded in 48-well plates at a concentration of 1×10^5 cells/ml. If needed, cells were infected by a retrovirus, as described above. After 24-h incubation, macrophages were seeded on the primary osteoblasts at a concentration of 1×10^5 cells/ml and treated with 10^{-8} M $1\alpha,25(OH)_2D_3$ and 10^{-6} M PGE_2 for 5 days. Osteoclasts were stained with tartrate-resistant acid phosphatase (3), and the cell number was counted. For separate culture, primary osteoblasts were cultured on the cell culture insert (BD Biosciences, San Jose, CA), and bone marrow macrophages were seeded on the bottom of 24-well plates.

Osteoclast Formation Assay by Soluble RANKL Generated by MMP14—293T cells were transfected with several combinations of pcDNA3.1-V5HisA, pcDNA3.1-RANKL-V5HisB, and pcDNA-mMMP14-V5HisA using FuGENE 6 (Roche Diagnostics, Indianapolis, IN), and 48 h after transfection, culture media were collected. Bone marrow macrophages were incubated with a 1:1 mixture of the culture media and α-MEM containing 10% FBS, supplemented with M-CSF at 10 ng/ml for 4 days.

Osteoclast Formation Assay, Survival Assay, and Pit Formation Assay of Macrophages of MMP14-deficient Mice—The MMP14-deficient mice were generated and backcrossed to the C57/BL6 strain as previously described (30). Livers and spleens were harvested from newborn MMP14-deficient mice and wild-type littermates, and cells were strained using a cell strainer. The obtained cells were incubated in α-MEM supplemented with 10% FBS, 1% penicillin-streptomycin solution, and 200 ng/ml M-CSF (Wako) for 4 days in 10-cm Petri dishes, and then M-CSF-dependent macrophages were recovered by trypsinization. For the osteoclast formation assay, macrophages were seeded in 48-well plates at a concentration of 2×10^5 cells/ml and treated with 10 ng/ml M-CSF and 100 ng/ml RANKL (Wako) for 6 days. For the survival assay and the pit formation assay, macrophages (2×10^5 cells/ml) were cocultured with primary osteoblasts (1×10^5 cells/ml) in α-MEM containing 10% FBS, 10^{-8} M $1\alpha,25(OH)_2D_3$, and 10^{-6} M PGE_2 on culture dishes precoated with 0.2% collagen gel matrix (Nitta Gelatin, Osaka, Japan). When osteoclasts were formed after 7-day culture, they were released from the dishes by treatment with 0.2% collagenase in phosphate-buffered saline, and collected by centrifugation. For the survival assay, cells were cultured on 48-well plates for 4 h, and osteoclasts were isolated by removing the osteoblasts by 0.1% collagenase and 0.2% dispase in phosphate-buffered saline. Purified osteoclasts were further incubated in α-MEM containing 10% FBS for 20 h. For the pit formation assay, cells were seeded on the dentin slices (Wako) precoated with FBS, and incubated in α-MEM containing 10% FBS, 10^{-8} M $1\alpha,25(OH)_2D_3$, and 10^{-6} M PGE_2 for 24 h. Then the cells were removed by ultrasonication after adding 1 M NH_4OH. Resorption pits were visualized by staining with 0.5% toluidine blue and analyzed using Adobe Photoshop (Adobe, San Jose, CA).

Histology—Tibias of 2- to 3-week-old male MMP14-deficient mice, and wild-type littermates were fixed in 4% paraformaldehyde and decalcified in 10% EDTA. Paraffin-embedded samples were sectioned at 5 μm and stained with hematoxylin and eosin or tartrate-resistant acid phosphatase. Observers who were blinded to the origin of the images counted the number of osteoclasts on the trabecular bone surface and measured total length of the trabecular bone using Image J software (National Institutes of Health, Bethesda, MD).

Statistical Analysis—Statistical analyses were performed using Student's *t* test for the alkaline phosphatase assay and a two-tailed unpaired Student's *t* test for the real-time PCR and ELISA. A *p* value of <0.05 was considered to be statistically significant.

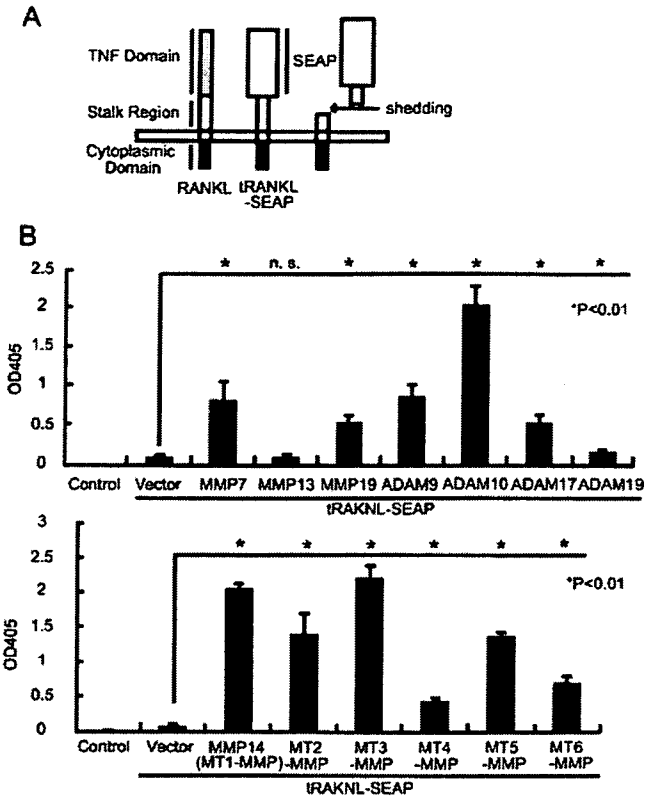

FIGURE 1. **RANKL shedding activity of MMPs and ADAMs.** *A*, schematic representation of RANKL and tRANKL-SEAP fusion protein. tRANKL-SEAP is a fusion protein of SEAP with C-terminally truncated RANKL, which contains the stalk region but lacks the TNF-like domain of RANKL, and with V5 and His× 6 tags at the C terminus. Cleavage of tRANKL-SEAP can be detected as positive alkaline phosphatase activity in the supernatants. *B*, alkaline phosphatase activity of the culture media of 293T cells transfected with pcDNA3.1-tRANKL-SEAP -V5HisA and expression vectors for ADAMs or MMPs ($n = 6$). *, significantly different, $p < 0.01$; *n. s.*, not significant.

RESULTS

Screening of MMPs and ADAMs as RANKL Sheddases—We previously developed a RANKL shedding activity screening system using an expression vector encoding a fusion protein of secreted placental alkaline phosphatase (SEAP) with the C-terminally truncated form of RANKL, which contains the stalk region, transmembrane domain, and intracellular domain of RANKL (tRANKL-SEAP) (20). Expression vectors of various MMPs or ADAMs were transfected to 293T cells together with tRANKL-SEAP plasmids, and the alkaline phosphatase activity of the culture media was measured. In this assay system, increased alkaline phosphatase activity in the medium indicates an increase in RANKL shedding (Fig. 1*A*). Several MMPs and ADAMs exhibited tRANKL-SEAP shedding activity, and ADAM10, MMP14 (membrane-type 1 matrix metalloproteinase, MT1-MMP), MT2, MT3, and MT5-MMP had relatively stronger activity (Fig. 1*B*). In contrast, MMP13 (Fig. 1*B*), MMP1, MMP2, MMP3, MMP9, MMP11, MMP23, and MMP28 (data not shown) had no tRANKL-SEAP shedding activity.

MMP14 and ADAM10 Are Major RANKL Sheddases in TM8B2 Cells—To confirm the ability of these proteinases to cleave full-length RANKL, they were overexpressed in the

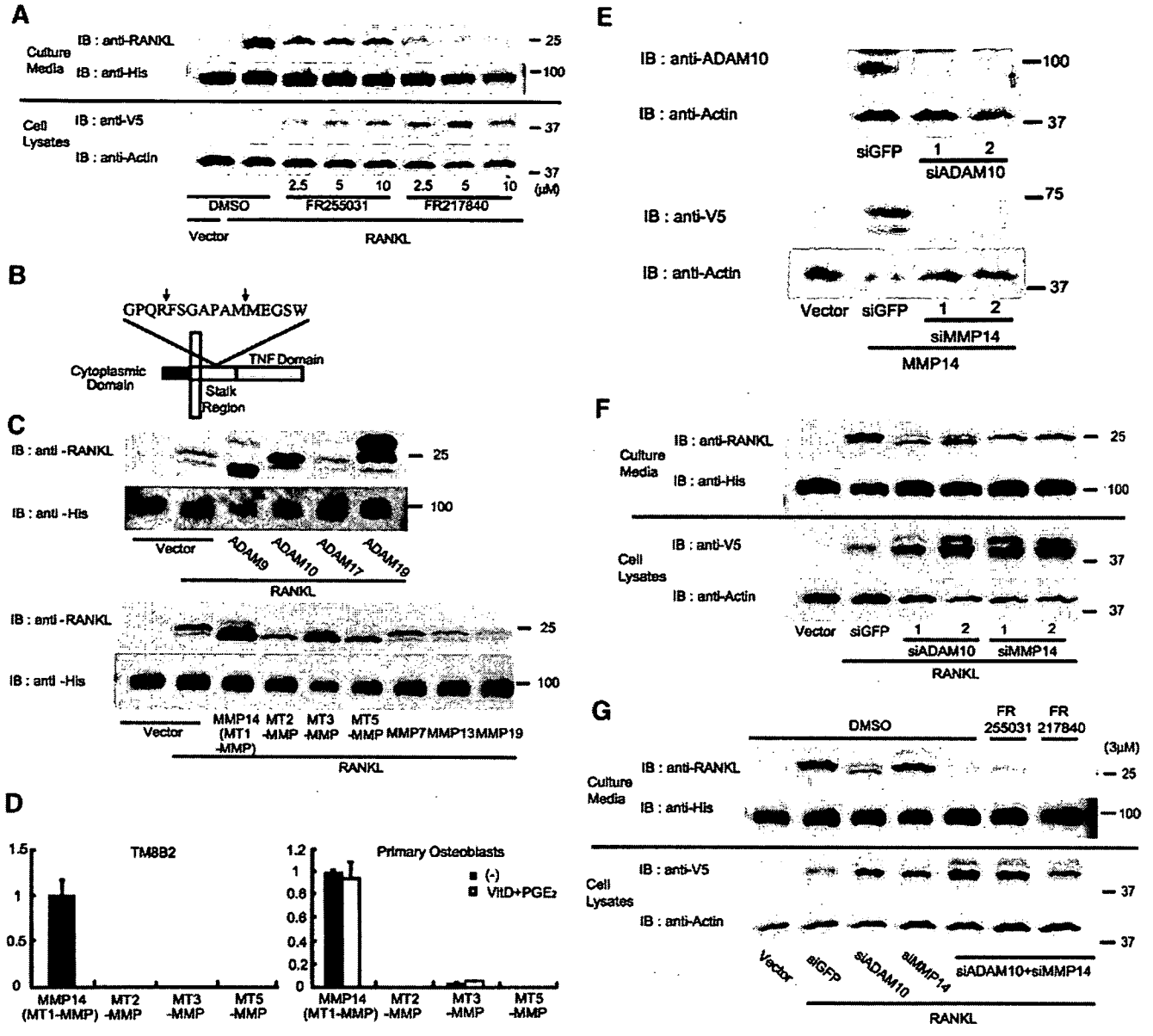

FIGURE 2. **ADAM10 and MMP14 are major RANKL sheddases in TM8B2 cells.** *A*, cleavage of full-length RANKL in TM8B2 cells transfected with pcDNA3.1-V5HisB or -RANKL. Twenty-four hours after transfection, culture media were changed to α-MEM containing either Me_2SO (*DMSO*), FR255031, or FR217840 together with 10% FBS. Culture media and cell lysates were subjected to Western blot analysis for RANKL after 72 h of incubation. Immunoblotting by anti-His shows the OPG-Fc recombinant protein used to collect soluble RANKL. *B*, schematic representation of the cleavage sites of RANKL. Cleavage sites were indicated by *arrows*. *C*, effect of ADAMs and MMPs on RANKL shedding in TM8B2 cells. TM8B2 cells were transfected with pcDNA3.1-RANKL-V5HisB and expression vectors for ADAMs or MMPs. Culture media were subjected to Western blot for RANKL 72 h after transfection. *D*, real-time PCR analysis of MT-MMP expression in TM8B2 cells and primary osteoblasts ($n = 3$). The *y*-axis represents the relative mRNA levels of the indicated genes expressed as -fold from MMP14 level. *E*, efficient gene knock-down by siADAM10 and siMMP14. TM8B2 cells were transfected with pcDNA3.1-V5HisA, piGENEmU6-siGFP, -siADAM10–1, -2, siMMP14–1, -2, or pcDNA3.1-mMMP14-V5HisA, and the expression of ADAM10 (endogenous) and MMP14 (overexpressed, detected by anti-V5 epitope tag antibody) was analyzed 48 h after transfection. *F*, Effect of siADAM10 and siMMP14 on RANKL cleavage in TM8B2 cells. TM8B2 cells were transfected with piGENEmU6-siGFP, -siADAM10–1, -2, siMMP14–1, -2, or pcDNA3.1-V5HisB, together with pcDNA3.1-RANKL-V5HisB. Seventy-two hours after transfection, culture media and cell lysates were collected and subjected to Western blot analysis. *G*, effects of siADAM10, siMMP14, and chemical inhibitors on RANKL shedding in TM8B2 cells. Procedures were the same as in *A*.

mouse bone marrow stromal cell line TM8B2 together with full-length RANKL. Soluble RANKL was recovered from the culture media using an OPG-Fc recombinant protein column and subjected to Western blot analysis. When RANKL (C-terminally tagged with V5 and 6× His) was overexpressed in TM8B2 cells (~39 kDa), there were two different molecular mass products (25 and 24 kDa) in the culture media (Fig. 2*A*). The N-terminal sequences of the two bands are shown in Fig. 2*B*. These two bands were differentially diminished by various metalloproteinase inhibitors (Fig. 2*A*). When TM8B2 cells were treated with FR255031, which inhibits several MMPs but not TNF-α secretases (31), only the lower band disappeared. On the other hand, treatment with FR217840, which not only inhibits several MMPs, but also inhibits TNF-α secretion (32), both of

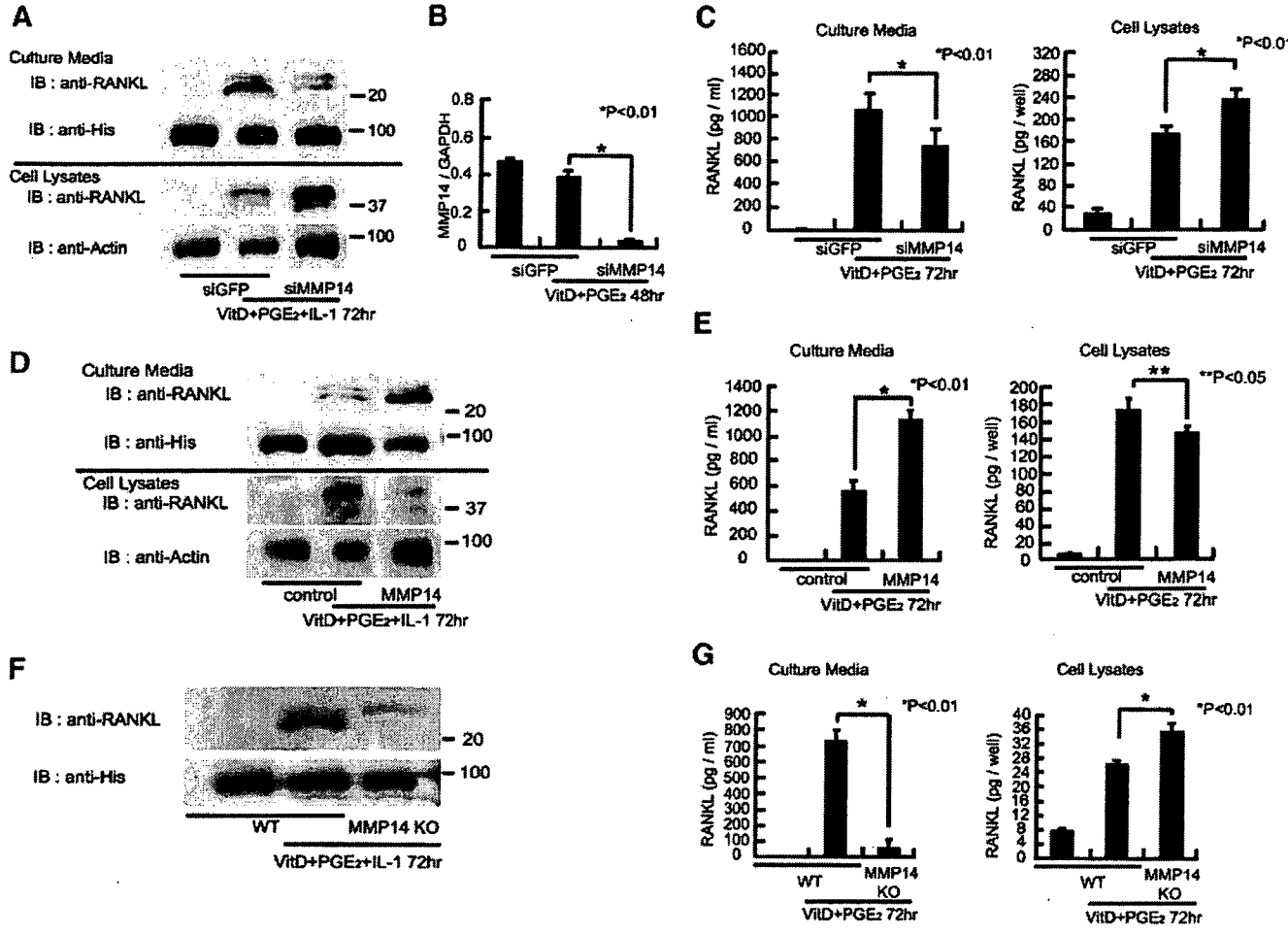

FIGURE 3. **MMP14 is a major RANKL sheddase in primary osteoblasts.** *A*, soluble and membrane-bound RANKL produced by primary osteoblasts infected with control or siMMP14 retrovirus. Twenty-four hours after infection, cells were untreated or treated with 10^{-8} M $1\alpha,25(OH)_2D_3$, 10^{-6} M PGE_2, and 10 ng/ml IL-1 for 72 h. Culture media and cell lysates were incubated with OPG-Fc fusion protein column, and the recovered proteins were subjected to Western blot analysis for RANKL. *B*, real-time PCR of MMP14 gene expression in primary osteoblasts infected with control or siMMP14 retrovirus ($n = 3$). *, significantly different, $p < 0.01$. *C*, RANKL concentration of culture media and cell lysates of primary osteoblasts as determined by ELISA ($n = 3$). Primary osteoblasts were infected with control or siMMP14 retrovirus. Twenty-four hours after infection, cells were untreated or treated with 10^{-8} M $1\alpha,25(OH)_2D_3$ and 10^{-6} M PGE_2 for 72 h. *, significantly different, $p < 0.01$. *D*, effects of retrovirus vector-mediated MMP14 overexpression on RANKL shedding in primary osteoblasts. Procedures were the same as in *A*. *E*, soluble (*left*) and membrane-bound (*right*) RANKL concentration produced by primary osteoblasts infected with control or MMP14 retrovirus ($n = 3$). Procedures were the same as in *C*. * and **, significantly different, $p < 0.01$ and $p < 0.05$, respectively. *F*, RANKL cleavage in primary osteoblasts from MMP14-deficient mice and the wild-type littermates. Cells were treated with or without 10^{-8} M $1\alpha,25(OH)_2D_3$, 10^{-6} M PGE_2, and 10 ng/ml IL-1 for 72 h. Culture media and cell lysates were incubated with osteoprotegerin-Fc fusion protein column, and the recovered proteins were subjected to Western blot analysis. *G*, RANKL concentration in culture media and cell lysates of primary osteoblasts from MMP14-deficient mouse and the wild-type littermate measured by ELISA ($n = 3$). Cells were treated with or without 10^{-8} M $1\alpha,25(OH)_2D_3$ and 10^{-6} M PGE_2 for 72 h. *, significantly different, $p < 0.01$.

the bands disappeared. These results suggest that the upper band is produced by ADAM family proteinase(s) and the lower band by MMP(s).

ADAM9, ADAM10, and ADAM19 cleaved full-length RANKL, but only ADAM10 produced soluble RANKL with the same molecular weight as the upper band observed in TM8B2 cells (Fig. 2*C*). ADAM17 did not cleave full-length RANKL. MMP14, MT2, MT3, and MT5-MMP generated soluble RANKL with the same molecular weight as the lower band. MT4- and MT6-MMP did not increase the soluble RANKL detected in the culture media (data not shown). Real-time PCR showed that the MMP14 mRNA level was much higher than that of MT2-, MT3-, or MT5-MMP in TM8B2 cells and primary osteoblasts (Fig. 2*D*), suggesting that MMP14 is mainly involved in the production of the lower band. The mRNA level of ADAM10 was comparable to that of MMP14 in these two cells (data not shown).

To determine the role of ADAM10 and MMP14 in the constitutive shedding of RANKL in TM8B2 cells, we constructed expression vectors of siRNA for ADAM10 and MMP14 (siADAM10 and siMMP14) (Fig. 2*E*). We constructed two different siADAM10 and siMMP14 vectors, and all of them effectively suppressed expression of the target molecules (Fig. 2*E*). The upper band of soluble RANKL diminished when the RANKL construct was transfected to TM8B2 cells along with siADAM10 plasmids; the lower band diminished with siMMP14 (Fig. 2*F*); and only the upper band was faintly observed when both siADAM10 and siMMP14 were transduced (Fig. 2*G*). The faint band completely disappeared in the presence of FR217840, but not FR255031 (Fig. 2*G*). These